17th International Conference on the Application of Computer
Science and Mathematics in Architecture and Civil Engineering
K. Gürlebeck and C. Könke (eds.)
Weimar, Germany, 12–14 July 2006

MULTIPHASE B-SPLINE FINITE ELEMENTS OF VARIABLE ORDER IN THE MECHANICAL ANALYSIS OF HETEROGENEOUS SOLIDS

S. Häfner*, M. Kessel and C. Könke

*Institute of Structural Mechanics, Bauhaus-University Weimar,
Marienstrasse 15, D-99423 Weimar, Germany
E-mail: stefan.haefner@bauing.uni-weimar.de

Keywords: multiphase, b-spline, finite element, heterogeneous solid.

Abstract. *Advanced finite elements are proposed for the mechanical analysis of heterogeneous materials. The approximation quality of these finite elements can be controlled by a variable order of B-spline shape functions. An element-based formulation is developed such that the finite element problem can iteratively be solved without storing a global stiffness matrix. This memory saving allows for an essential increase of problem size. The heterogeneous material is modeled by projection onto a uniform, orthogonal grid of elements. Conventional, strictly grid-based finite element models show severe oscillating defects in the stress solutions at material interfaces. This problem is cured by the extension to multiphase finite elements. This concept enables to define a heterogeneous material distribution within the finite element. This is possible by a variable number of integration points to each of which individual material properties can be assigned. Based on an interpolation of material properties at nodes and further smooth interpolation within the finite elements, a continuous material function is established. With both, continuous B-spline shape function and continuous material function, also the stress solution will be continuous in the domain. The inaccuracy implied by the continuous material field is by far less defective than the prior oscillating behaviour of stresses. One- and two-dimensional numerical examples are presented.*

1 INTRODUCTION

1.1 Background of grid-based modeling

Grid-based procedures for the finite element analysis of concrete as heterogeneous material on the mesoscale have been presented in [4, 5]. These procedures include geometrical modeling of the heterogeneous material, efficient grid-based notation of the finite element problem and the multigrid method as fast iterative solver method to the defined problem. These priorly proposed methods are efficient in memory demand as well as computational cost and therefore are appropriate to analyze the material behaviour of heterogeneous solids by a very large number of degrees of freedom [5, 8]. The effective elastic properties of various complex mesoscale geometries of concrete models were computed and verified by experimental results [5]. However, while the application of grid-based models, also labeled as pixel or voxel models, is quite comfortable and efficient for geometrical modeling of heterogeneous solids and concerning numerical methods, the inadequate grid-based representation of inclusion interfaces leads to severely defective stress solutions. Besides other possible solutions [7], the present approach of multiphase B-spline finite elements is introduced to tackle this problem.

1.2 B-spline finite elements and multiphase finite elements

The present paper introduces a combination of B-spline finite elements with the multiphase finite element concept. In the following the major references for the development of this approach are introduced. The mathematical theory of B-spline finite elements is prepared in *Höllig* [10]. It includes so-called web-splines (weighted extended B-splines) for modeling of curved domains. The corresponding method is applied to various physical applications such as in the computation of a stationary temperature distribution, the velocity of an incompressible flow and the deformation of linear elastic bodies. However, while the domains are variable in shape they are principally homogeneous. The present approach only considers rectangular domains, but it is designed to model heterogeneous material inside the domain. A possible application of this approach is the mechanical analysis of heterogeneous materials on the mesoscale where the macroscopic shape of the analyzed body is not of importance.

Multiphase finite elements are presented in *Steinkopff, Sautter & Wulf* [18] and *Zohdi* [21]. Besides several other advanced finite elements methods [16], multiphase finite elements provide an interesting alternative to model heterogeneous materials. Arbitrary geometries of the heterogeneous material can be mapped on the integration points of e.g. a uniform orthogonal mesh of finite elements. Generally this method is expected to be less accurate than aligned meshing. However, this method only requires pointwise information of the material. Therefore it is convenient for modeling very complex heterogeneous materials even by three-dimensional models [4].

The method presented in this paper integrates the multiphase finite element concept into B-spline finite elements of variable order k while the stated advantages of grid-based modeling (Section 1.1) can principally be maintained. As a result, the combination of high-performance and improved accuracy lead to a new quality in grid-based modeling of heterogeneous materials.

1.3 Outline and key aspects of present approach

Section 2 summarizes the boundary value problem of linear elasticity and introduces to the applied notation. By means of the principle of virtual displacements, the classical displacement-based finite element formulation is provided in Section 3. Relevant aspects with regard

to B-spline finite elements are included. Section 4 introduces to univariate splines and B-splines. As a relevant key aspect specific modified B-splines according to *Schwetlick & Kretzschmar* [17] are introduced which will allow for a comfortable definition of displacement boundary conditions. A transparent introduction to one-dimensional B-spline finite elements is provided in Section 5. As an important aspect, the B-splines are splitted to form individual finite elements which are assigned to one grid cell as presented in *Kessel* [13]. The analysis is exemplified for two problems of a homogeneous bar. These examples are comprehensible by hand calculation and provide clear access to this method.

In Section 6 two-dimensional B-spline finite elements of variable order k are introduced. It includes the Gauss-Legendre numerical integration for polynomials of variable order as given in *Duschek* [3], the formulation of the global stiffness problem, the definition of boundary conditions and an adaption to iterative solving methods without storage of a global stiffness matrix. Corresponding implementation issues are discussed in *Kessel* [14]. A two-dimensional homogeneous test problem with higher-order polynomial loading establishes a verification of the implemented method. The convergence rates of relative error in energy are analyzed with respect to order k of elements (p-version) and size of elements (h-version) in comparison to classical error estimates provided in *Zienkiewicz & Taylor* [19].

Section 7 introduces to the proposed multiphase finite element concept to model heterogeneous materials. The mechanical theory of a material discontinuity is outlined. In the idea of this approach the original mechanical problem is transformed into a substitute problem with continuous material function. While the B-spline finite elements showed severe local defects for the original problem, they are well applicable to the substitute problem. The accuracy of the substitute problem can be scaled by one parameter s_t and in the theoretical limit state $s_t \longrightarrow 0$ the substitute problem converges to the original problem. After a corresponding introduction to multiphase finite elements, a simple bar example highlights the effect of transforming the mechanical problem. Two further examples deal with a circular inclusion in a matrix. A plain grid discretization of the circle and an exact mapping of the transformed problem are presented and analyzed with respect to the defect in the stress solution. Another example of only one material transition establishes a thorough analysis of the multiphase B-spline finite element method with regard to type of transition function of the substitute problem, order of elements and size of elements. Similar to the homogeneous problem an error analysis in terms of stresses and energy follows. Finally also an effective overall error is estimated. This allows to identify optimal parameter combinations of the presented method and supplies evidence of its potential.

2 FUNDAMENTALS OF LINEAR ELASTICITY

2.1 Three-dimensional linear elastic problem

An elastic three-dimensional body in a Cartesian coordinate system with base vectors $\boldsymbol{e}_i$, with $i = 1, 2, 3$, is considered. In the view of continuum mechanics the body is continuous as well as all corresponding vector fields, such as displacements $\boldsymbol{U} = U_i\, \boldsymbol{e}_i$, strains $\boldsymbol{\epsilon} = \epsilon_{ij}\, \boldsymbol{e}_i \otimes \boldsymbol{e}_j$ and stresses $\boldsymbol{\sigma} = \sigma_{ij}\, \boldsymbol{e}_i \otimes \boldsymbol{e}_j$. For the linearized theory it is unique to introduce only one coordinate system. In an initial, undeformed state a material point of the body is located at position $\boldsymbol{X} = X_i\, \boldsymbol{e}_i$. All field variables refer to this initial configuration and thus can be considered as a function of $\boldsymbol{X}$: $\boldsymbol{U} = \boldsymbol{U}(\boldsymbol{X})$, $\boldsymbol{\epsilon} = \boldsymbol{\epsilon}(\boldsymbol{X})$ and $\boldsymbol{\sigma} = \boldsymbol{\sigma}(\boldsymbol{X})$. Due to the following symmetry[1] of

[1]For this symmetry the general absence of body moments is presumed.

strain coordinates $\epsilon_{ij} = \epsilon_{ji}$ and stress coordinates $\sigma_{ij} = \sigma_{ji}$, the elastic problem includes 15 unknown variables in the coordinates of $\boldsymbol{U}$, $\boldsymbol{\epsilon}$ and $\boldsymbol{\sigma}$; respectively $3 + 6 + 6 = 15$. As a formal solution to determine these unknown state variables a system of 15 equations is introduced, while as well predefined displacements and tractions on the surface of the body need to be satisfied. This describes the elliptic boundary value problem of linear elasticity. Six kinematic equations

$$\boldsymbol{\epsilon} = \frac{1}{2}\left(\operatorname{grad}\boldsymbol{U} + (\operatorname{grad}\boldsymbol{U})^{\mathrm{T}}\right) , \qquad \epsilon_{ij} = \frac{1}{2}\left(U_{i,j} + U_{j,i}\right) \tag{2.1}$$

define the relationship of strains $\boldsymbol{\epsilon}$ and displacements $\boldsymbol{U}$. Six constitutive equations

$$\boldsymbol{\sigma} = \mathbb{C}\,\boldsymbol{\epsilon} , \qquad \sigma_{ij} = C_{ijkl}\,\epsilon_{kl} \tag{2.2}$$

couple stresses $\boldsymbol{\sigma}$ and strains $\boldsymbol{\epsilon}$ where in the case of the generalized Hooke's law for homogeneous, isotropic material the material tensor C_{ijkl} is defined as

$$C_{ijkl} = \lambda\,\delta_{ij}\,\delta_{kl} + \mu\,\left(\delta_{ik}\,\delta_{jl} + \delta_{il}\,\delta_{jk}\right) \tag{2.3}$$

It is noted that the Einstein summation convention defines summation over repeated indices. The Kronecker delta δ_{ij} is equal to 1 for $i = j$ and equal to 0 for $i \neq j$. The material specific variables μ and λ are the Lame constants. The Lame constants can be substituted by Young's Modulus E and Poisson's ratio ν. The corresponding conversions are

$$\mu = \frac{E}{2(1+\nu)} , \quad \lambda = \frac{\nu E}{(1+\nu)(1-2\nu)} , \quad E = \frac{\mu\,(2\mu + 3\lambda)}{\mu + \lambda}, \quad \nu = \frac{\lambda}{2\,(\mu + \lambda)} \tag{2.4}$$

Equilibrium is described by the following three equations

$$\int_V p_i dV + \int_A \sigma_{ji} n_j dA = 0 \tag{2.5}$$

which mean that, in total, body forces $p_i \boldsymbol{e}_i$ and surface tractions $\sigma_{ji} n_j \boldsymbol{e}_i$ of any considered volume V, which is bounded by the surface area A, vanish. By the divergence theorem this equation is transformed into the following well-known fundamental strong form of equilibrium

$$\operatorname{div}\boldsymbol{\sigma} + \boldsymbol{p} = \boldsymbol{0} , \qquad \sigma_{ji,j} + p_i = 0 \tag{2.6}$$

The analytical solution requires a state of equilibrium at any point on the surface and within the volume of the considered body. The body is fixed to avoid rigid body motion. It is loaded by body loads $\boldsymbol{p} = p_i\,\boldsymbol{e}_i$ and surface tractions $\boldsymbol{t} = t_i\,\boldsymbol{e}_i$. The surface tractions at the boundary of the body correspond to the adjacent stresses $t_i\,\boldsymbol{e}_i = \sigma_{ji} n_j \boldsymbol{e}_i$ where n_j are the components of the outward oriented normal unit vector $\boldsymbol{n} = n_j\,e_j$. It is a boundary value problem with prescribed displacements $\boldsymbol{U}_D$ on Γ_D and prescribed surface tractions $\boldsymbol{t}$ on Γ_N

$$\boldsymbol{U} = \boldsymbol{U}_D \quad \text{on } \Gamma_D \tag{2.7}$$

$$\boldsymbol{\sigma}\,\boldsymbol{n} = \boldsymbol{t} \quad \text{on } \Gamma_N \tag{2.8}$$

The solution is unique, if rigid body modes are excluded and under some further assumptions, which generally apply to engineering models (e.g. Young's modulus is positive).

2.2 Two- and one-dimensional linear elastic problem

Under certain conditions and presumptions a three-dimensional elasticity problem can be reduced to a two-dimensional problem. For example, labels of such special states are plane stress, plane strain or axisymmetric. In this paper only the plane stress state is considered. For plane stress parallel to the X_1X_2-plane, the stress components σ_{13}, σ_{23} and σ_{33} are equal to zero. The other stress components are constant with respect to X_3. The kinematics equation and the equilibrium equation can directly be reduced to two-dimensional by reducing the range of the indices i and j to 2. The constitutive relationship in the plane stress state is

$$\sigma_{11} = \frac{E}{(1-\nu^2)}\left(\epsilon_{11} + \nu\epsilon_{22}\right) , \qquad \sigma_{22} = \frac{E}{(1-\nu^2)}\left(\nu\epsilon_{11} + \epsilon_{22}\right) , \qquad \sigma_{12} = \frac{E}{2\,(1+\nu)}\gamma_{12} \tag{2.9}$$

with $\gamma_{12} = 2\epsilon_{12}$ according to Eq. 2.1. A reduction to one dimension as to the uniaxial stress problem corresponds to the typical model of a bar. All stress components except σ_{11} are equal to zero. In this case the kinematics equation, constitutive equation and equilibrium equation are

$$\epsilon_{11} = U_{1,1} , \qquad \sigma_{11} = E\epsilon_{11} , \qquad \sigma_{11,1} + p_1 = 0 \tag{2.10}$$

3 FINITE ELEMENTS FOR MECHANICAL ANALYSIS

3.1 Principle of virtual displacements

Based on the stated boundary value problem of elasticity the principle of virtual displacements can be derived, as e.g. shown in *Bathe* [1]. Assuming a body in equilibrium the principle of virtual displacements states that for any virtual displacements $\delta\boldsymbol{U}$, which are conform to the displacement boundary conditions, the total internal virtual work (l.h.s.) is equal to the total external virtual work (r.h.s.).

$$\int_\Omega \delta\boldsymbol{\epsilon}^{\mathrm{T}}\boldsymbol{\sigma}dV = \int_\Omega \delta\boldsymbol{U}^{\mathrm{T}}\boldsymbol{p}_b\, dV + \int_{\Gamma_N} \delta\boldsymbol{U}^{\mathrm{T}}\boldsymbol{p}_s\, dA \tag{3.1}$$

The virtual displacements $\delta\boldsymbol{U}$ must be continuous and vanish at the surface of prescribed displacements Γ_D. The virtual strains $\delta\boldsymbol{\epsilon}$ are directly related to the virtual displacements $\delta\boldsymbol{U}$ according to Equation 2.1. The external virtual work is induced by body loads $\boldsymbol{p}_b$ and surface loads $\boldsymbol{p}_s$. The principle of virtual displacements is the basis of the displacement-based finite element formulation.

3.2 Displacement-based finite elements for mechanical analysis

A linear elastic, continuous body is considered according to the stated three-, two- or one-dimensional boundary value problem of elasticity. For finite element approximation the continuum is divided into a finite number of parts, which will be labeled as finite elements. These elements are interconnected at nodes. Therefore the continuous problem is transformed into a discrete problem with a finite number of degrees of freedom. The interpretation of degrees of freedom as nodal values is only valid for classical finite elements, but not for B-spline finite elements (except for B-splines of order k=1). However, the property remains that a degree of freedom is a factor which is assigned to a shape function such that the principal interpolation rule remains.

The degrees of freedom are stored in a global vector $\boldsymbol{u}$ in a predefined order. To each element a local order of degrees of freedom is assigned. For each element e an individual matrix of shape functions $\boldsymbol{N}^e$ defines the displacement interpolation field $\boldsymbol{U}^e$ within the volume V^e of this element as a function of degrees of freedom $\boldsymbol{u}^e$ of this element

$$\boldsymbol{U}^e = \boldsymbol{N}^e \boldsymbol{u}^e \,, \qquad U_i^e = N_{ij}^e u_j^e \tag{3.2}$$

where i counts from 1 to the dimension of the stated boundary value problem (1,2 or 3) and j counts through all local degrees of freedom of element e. The displacement field as a continuous function within the element e enables to apply the kinematics (Eq. 2.1) and leads to

$$\boldsymbol{\epsilon}^e = \boldsymbol{B}^e \boldsymbol{u}^e \,, \qquad \epsilon_k^e = B_{kj}^e u_j^e \tag{3.3}$$

where $\boldsymbol{B}^e$ defines the strain-displacement matrix and k refers to the number of strain components of vector $\boldsymbol{\epsilon}^e$. The material matrix C establishes a unique relationship between stresses $\boldsymbol{\sigma}^e$ and strains $\boldsymbol{\epsilon}^e$

$$\boldsymbol{\sigma}^e = \boldsymbol{C}^e \boldsymbol{\epsilon}^e \,, \qquad \sigma_k^e = C_{kl}^e \epsilon_l^e \tag{3.4}$$

with both variables k and l in the range of 1 to 6 for the three-dimensional case. Then, the finite element definitions (Eqs. 3.2-3.4) of discretized state variables adopted by the principle of virtual displacements (Eq. 3.1) for one element e yield[2]

$$\int_{V^e} \delta \boldsymbol{u}^{e\mathrm{T}} \boldsymbol{B}^{e\mathrm{T}} \boldsymbol{C}^e \boldsymbol{B}^e \; \boldsymbol{u}^e dV = \int_{V^e} \delta \boldsymbol{u}^{e\mathrm{T}} \boldsymbol{N}^{e\mathrm{T}} \boldsymbol{p}_b^e \; dV + \int_{A^e} \delta \boldsymbol{u}^{e\mathrm{T}} \boldsymbol{N}^{e\mathrm{T}} \boldsymbol{p}_s^e \; dA \tag{3.5}$$

As the entries of the vectors $\boldsymbol{u}^e$ and $\delta \boldsymbol{u}^e$ are not functions in V^e or A^e, but constants, these vectors can both be extracted from the integral, which further allows for a complete elimination of $\delta \boldsymbol{u}^e$. This results in the following fundamental relationship

$$\boldsymbol{K}^e \boldsymbol{u}^e = \boldsymbol{f}^e \tag{3.6}$$

for one element, where $\boldsymbol{K}^e$ is the element stiffness matrix with

$$\boldsymbol{K}^e = \int_{V^e} \boldsymbol{B}^{e\mathrm{T}} \boldsymbol{C}^e \boldsymbol{B}^e \; dV \tag{3.7}$$

and $\boldsymbol{f}^e$ is the vector of nodal forces

$$\boldsymbol{f}^e = \int_{V^e} \boldsymbol{N}^{e\mathrm{T}} \boldsymbol{p}_b^e dV + \int_{A^e} \boldsymbol{N}^{e\mathrm{T}} \boldsymbol{p}_s^e dA \tag{3.8}$$

under the implied presumption that the functions of body loads $\boldsymbol{p}_b^e$ and surface loads $\boldsymbol{p}_s^e$ are given in the same local coordinate system as the interpolation matrix $\boldsymbol{N}^e$. In Equation 3.6 the unknown variables are the degrees of freedom of the displacement vector $\boldsymbol{u}^e$ as defined beforehand. Globally the principle of virtual displacements yields the global equation system

$$\boldsymbol{K}\boldsymbol{u} = \boldsymbol{f} \tag{3.9}$$

where the global stiffness matrix corresponds to the sum of element stiffness matrices $\bar{\boldsymbol{K}}_e$ after rearrangement according to the global degrees of freedom

$$\boldsymbol{K} = \sum_{e=1}^{n^e} \bar{\boldsymbol{K}}^e \,, \qquad K_{ij} = \sum_{e=1}^{n^e} \bar{K}_{ij}^e \tag{3.10}$$

[2]For two matrices $\boldsymbol{A}$ and $\boldsymbol{B}$ the equality $(\boldsymbol{AB})^{\mathrm{T}} = \boldsymbol{B}^{\mathrm{T}} \boldsymbol{A}^{\mathrm{T}}$ is recalled.

and the global force vector corresponds to the sum of reordered element force vectors $\bar{\boldsymbol{f}}^e$.

$$\boldsymbol{f} = \sum_{e=1}^{n^e} \bar{\boldsymbol{f}}^e \,, \qquad f_i = \sum_{e=1}^{n^e} \bar{f}_i^e \tag{3.11}$$

However, the element stiffness matrix $\boldsymbol{K}^e$ as in Equation 3.6 is singular and therefore the solution of the displacement vector $\boldsymbol{u}^e$ is not unique. Displacement boundary conditions need to be integrated into the finite element scheme. Considering all global degrees of freedom of a finite element model, then here the index 1 corresponds to degrees of freedom with a prescribed force and the index 2 corresponds to those of a prescribed displacement.

$$\begin{bmatrix} \boldsymbol{K}_{1,1} & \boldsymbol{K}_{1,2} \\ \boldsymbol{K}_{2,1} & \boldsymbol{K}_{2,2} \end{bmatrix} \begin{bmatrix} \boldsymbol{u}_1 \\ \boldsymbol{u}_2 \end{bmatrix} = \begin{bmatrix} \boldsymbol{f}_1 \\ \boldsymbol{f}_2 \end{bmatrix} \tag{3.12}$$

The initially unknowns of this system are $\boldsymbol{u}_1$ and $\boldsymbol{f}_2$. As the right hand side of the following equation is known, it is possible to compute $\boldsymbol{u}_1$

$$\boldsymbol{K}_{1,1}\, \boldsymbol{u}_1 = \boldsymbol{f}_1 - \boldsymbol{K}_{1,2}\, \boldsymbol{u}_2 \tag{3.13}$$

independent of $\boldsymbol{f}_2$. For further interest the resulting force vector $\boldsymbol{f}_2$ at rigid degrees of freedom yields

$$\boldsymbol{f}_2 = \boldsymbol{K}_{2,1}\, \boldsymbol{u}_1 + \boldsymbol{K}_{2,2}\, \boldsymbol{u}_2 \tag{3.14}$$

4 DESCRIPTION OF B-SPLINES

4.1 Fundamentals of univariate splines

Univariate means that the spline is one-dimensional or a function of one variable, here x. For the definition of a univariate spline $\bar{s}$ in the interval $[x_0, x_n]$ a sequence of supporting points x_i is introduced with the condition that

$$x_i < x_{i+1} \qquad \text{for} \quad i = 0, \ldots, n-1. \tag{4.1}$$

A spline function $\bar{s}$ of order k is composed of piecewise polynomials $\bar{p}_i$ for $i = 0, \ldots, (n-1)$ where each polynomial $\bar{p}_i$ is at maximum of order k. The piecewise polynomials $\bar{p}_i$ have limited support in the interval $[x_0, x_n]$ and are defined as

$$\bar{p}_i(x) = \begin{cases} \sum_{j=0}^{k} \bar{c}_{i,j}\, x^j & \text{for } x \in [x_i; x_{i+1}) \\ 0 & \text{for } x \notin [x_i; x_{i+1}) \end{cases} \tag{4.2}$$

with $k \geq 1$. The coefficients $\bar{c}_{i,j}$ are scalar values which define the piecewise polynomial $\bar{p}_i$. In addition to the given function the last piecewise polynomial $\bar{p}_{n-1}$ also includes the upper boundary value x_n to close the spline interval $[x_0, x_n]$. Therewith the spline $\bar{s}$ is defined as

$$\bar{s}(x) = \sum_{i=0}^{n-1} \bar{p}_i(x) \qquad \text{for} \quad x \in [x_0, x_n] \tag{4.3}$$

The coordinates x_i for $i = 1, \ldots, (n-1)$ where the polynomials join are labeled as breaking points. In the complete interval $[x_0, x_n]$ the spline $\bar{s}$ has $(k-r)$ continuous derivatives. This

property is declared as C^{k-r}-continuity. While each piecewise polynomial $\bar{p}_i$ is naturally C^k-continuous in the interval $[x_i, x_{i+1}[$, the continuity of the spline is only reduced at the breaking points by a predefined order $r \geq 1$. Otherwise, if $r = 0$ at all breaking points the spline would be one polynomial over the whole interval.

The prior definitions provide some basic fundamentals of splines. However, it is noted that the provided information is not sufficient for a practical application as e.g. in the approximation of an unknown function only by a given sequence $x_0 \dots x_n$ of supporting points. For splines of higher order ($k \geq 2$) there are more polynomial coefficients to determine than conditions are given by the definitions above. For example, for splines of order $k = 2$, one additional condition needs to be specified, such as the minimization of the second order derivative, an additional value of the function or its derivative, while various choices lead to various approximation quality. This problem continues with increasing order k. An extensive mathematical theory treats many special properties and methods related to various forms of splines. The subsequent introduction is restricted to B-splines (basis splines), which as a sub-category of splines, also satisfy the given fundamentals.

4.2 B-splines as a functional basis of splines

In comparison to Equation 4.3 any C^{k-1} continuous spline of order k can also be defined as linear combination of $n + k$ linear independent B-splines b_j^k

$$\bar{s}(x) = \sum_{j=-k}^{n-1} c_j b_j^k(x) \qquad \text{for} \quad x \in [x_0, x_n] \tag{4.4}$$

The coefficients c_j are the corresponding scalar values. It can simply be shown that there exist exactly $n + k$ linear independent B-splines in the interval $[x_0, x_n]$. For the definition of each segment of a spline or piecewise polynomial $(k + 1)$ coefficients have to be defined. On the whole interval this results in $n(k + 1) = nk + n$ coefficients. Presuming C^{k-1} continuity, at each of $(n - 1)$ breaking points k continuity conditions have to be satisfied which leads to $(n - 1)k = nk - k$ conditions. Therewith $(nk + n) - (nk - k) = n + k$ parameters can be determined to define a certain spline.

B-splines of order k form a spline basis which always satisfies the intrinsic spline conditions while the choice of $(n + k)$ parameters c_j allows to define any C^{k-1} continuous spline. A B-spline has only support on $k + 1$ neighbouring intervals such that

$$b_j(x) = 0 \qquad \text{for} \quad x \notin [x_j, x_{j+k+1}] \tag{4.5}$$

Therewith Equation 4.4 can be rewritten as

$$\bar{s}(x) = \sum_{j=i-k}^{i} c_j b_j^k(x) \qquad \text{for} \quad x \in [x_i, x_{i+1}] \;\text{ and }\; i = 0 \dots n-1 \tag{4.6}$$

which means that in the interval $[x_i, x_{i+1}]$ there will be $(k + 1)$ B-splines defined. Equation 4.6 yields that the considered spline interval $[x_0, x_n]$ also includes B-Splines of the intervals $[x_{-k}, x_1]$ and $[x_{n-1}, x_{n+k}]$.

4.3 B-spline formulations

The uniform B-spline b^k of order k is defined by the recursion

$$b^k(x) = \int_{x-1}^{x} b^{k-1}(t)\mathrm{d}t \tag{4.7}$$

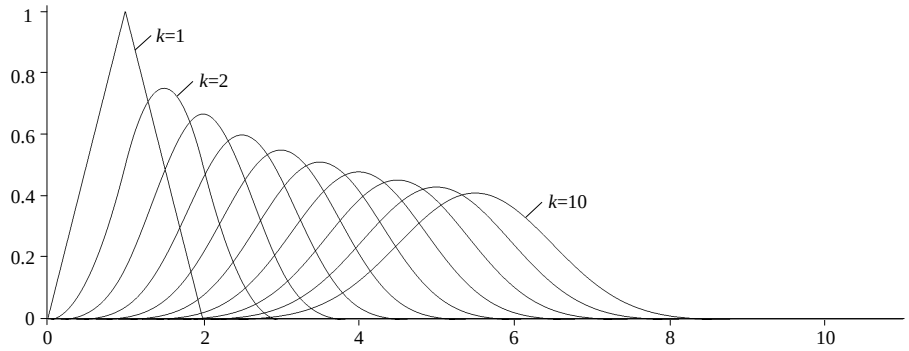

Fig. 4.1: Uniform B-splines of order $k = 1 \dots 10$

starting from the characteristic function b^0 of the unit interval [0;1]

$$b^0(x) = \begin{cases} 1 & \text{for } x \in [0;1) \\ 0 & \text{for } x \notin [0;1) \end{cases} \tag{4.8}$$

Alternatively, for computational reasons Equation 4.7 can be brought into the following form, labeled as Recurrence Relation [2, 10]

$$b^k(x) = \frac{x}{k} b^{k-1}(x) + \frac{k+1-x}{k} b^{k-1}(x-1) \tag{4.9}$$

The application of the recursion of Equation 4.7 to the constant B-Spline (Eq. 4.8) yields the uniform, linear B-spline

$$b^1(x) = \begin{cases} x & \text{for } x \in [0;1) \\ -x+2 & \text{for } x \in [1;2) \\ 0 & \text{otherwise} \end{cases} \tag{4.10}$$

which is also known as hat-function within the context of finite elements. The same principle then leads to the uniform quadratic B-spline

$$b^2(x) = \begin{cases} \frac{1}{2}x^2 & \text{for } x \in [0;1) \\ -x^2 + 3x - \frac{3}{2} & \text{for } x \in [1;2) \\ \frac{1}{2}x^2 - 3x + \frac{9}{2} & \text{for } x \in [2;3) \\ 0 & \text{otherwise} \end{cases} \tag{4.11}$$

and the uniform cubic B-spline.

$$b^3(x) = \begin{cases} \frac{1}{6}x^3 & \text{for } x \in [0;1) \\ -\frac{1}{2}x^3 + 2x^2 - 2x + \frac{2}{3} & \text{for } x \in [1;2) \\ \frac{1}{2}x^3 - 4x^2 + 10x - \frac{22}{3} & \text{for } x \in [2;3) \\ -\frac{1}{6}x^3 + 2x^2 - 8x + \frac{32}{3} & \text{for } x \in [3;4) \\ 0 & \text{otherwise} \end{cases} \tag{4.12}$$

The first ten B-splines of order $k = 1 \dots 10$ are shown in Figure 4.1. The uniform B-Spline of order k is of the length $k + 1$. The uniform B-Spline is scaled to a segment length h and translated by a distance d by the following expression.

$$b^k_{d,h}(x) = b^k(x/h - d) \tag{4.13}$$

Considering an infinite sequence of similar B-splines at a neighbouring distance $d = h$, the sum of these B-splines will be equal to 1 at any coordinate (partition of unity). It also follows that in each interval $[x_i, x_{i+1}]$, with $x_{i+1} = x_i + h$, similar B-spline segments will be represented. For the following formulation of B-spline finite elements it will be useful and sufficient only to consider these $(k+1)$ B-Spline functions in an interval $[0, h]$.

4.4 Modified B-Splines towards Endpoints

For the following finite element approach it is advantageous to modifiy the B-splines such that the endpoints of the spline will either be equal to 0 or to 1. Then it will be straightforward to apply displacement boundary conditions. Therefore a special recurrence relation, as presented in *Schwetlick & Kretzschmar* [17], will be adapted. It starts by the following definition of B-splines of order $k = 1$.

$$b_j^1(x) = \begin{cases} \frac{x - x_j}{x_{j+1} - x_j} & \text{for } x \in [x_j; x_{j+1}) \\ \frac{x_{j+2} - x}{x_{j+2} - x_{j+1}} & \text{for } x \in [x_{j+1}; x_{j+2}) \\ 0 & \text{otherwise} \end{cases} \tag{4.14}$$

Multiple knots will be introduced at the coordinates of the endpoints in the considered interval $[x_0; x_n]$.

$$x_{-k} = x_{-k+1} = \ldots = x_{-1} = x_0 \quad , \quad x_n = x_{n+1} = \ldots = x_{n+k-1} = x_{n+k} \tag{4.15}$$

The modified B-Splines of order $k > 1$ can recursively developed by

$$b_j^k = \omega_j^{k-1}(x) b_j^{k-1}(x) + [1 - \omega_{j+1}^{k-1}(x)] b_{j+1}^{k-1}(x) \tag{4.16}$$

with

$$\omega_j^{k-1}(x) = \begin{cases} \frac{x - x_j}{x_{j+k} - x_j} & \text{if} \quad x_{j+k} > x_j \\ 0 & \text{if} \quad x_{j+k} = x_j \end{cases} \tag{4.17}$$

for $j = -k, \ldots, n-1$. This recursive formula is designed to develop (modified) B-splines in the interval $[x_0; x_n]$. For implementation issues it is referred to *Kessel* [14]. Modified B-splines segments occur in $(k-1)$ intervals (of length h) towards the endpoints. This means that in $(2k-1)$ intervals, one regular B-spline segment will be created in the center. A larger number of intervals leads to several regular B-spline segments in the center. A smaller interval causes to create modified B-splines only. For the case of $k = 2$, three segments are required to include exactly one regular B-spline. Figure 5.1 shows such modified and regular B-splines of order $k = 2$ in the interval $[x_0, x_4]$. The various occuring B-spline types in one interval according to Figure 5.1 are highlighted in detached form in Figure 5.2.

5 ONE-DIMENSIONAL B-SPLINE FINITE ELEMENTS

As descriptive demonstration of B-spline finite elements the one-dimensional case is included. The corresponding formulation is explicitely given for quadratic B-spline finite elements. This Section prepares some basic principles for the following more abstract and symbolic description of two-dimensional B-spline finite elements in Section 6.

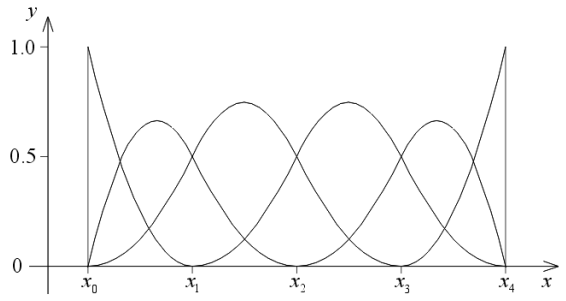

Fig. 5.1: Partition of unity by 6 B-splines (k=2) which are modified in the end segments (x_0, x_1) and (x_3, x_4) .

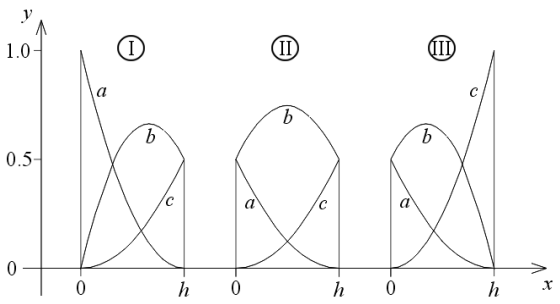

Fig. 5.2: B-splines (k=2) splitted into finite elements (I,II,III) with three shape functions (a,b,c) each.

5.1 Local interpolation scheme

As a special characteristic about the following formulation of B-spline finite elements, the B-splines are splitted into segments to create element stiffness matrices for each interval separately. Nevertheless, continuity of the displacement solution will be recovered by a specific assembly of the global stiffness matrix. The interpolation of the displacements (Eq. 3.2) is defined by $\boldsymbol{N}^J$ where J is a placeholder for the different element types I, II or III according to Figure 5.2 by

$$U(x) = \boldsymbol{N}^J \boldsymbol{u} \tag{5.1}$$

with the following degrees of freedom

$$\boldsymbol{u} = \left[\begin{array}{ccc} u_a & u_b & u_c \end{array} \right]^{\mathrm{T}} \tag{5.2}$$

and the interpolation functions, or shape functions, $\boldsymbol{N}^J$

$$\begin{array}{rcl} \boldsymbol{N}^I & = & \left[\begin{array}{ccccc} \frac{x^2}{h^2} - \frac{2x}{h} + 1 & , & -\frac{3x^2}{2h^2} + \frac{2x}{h} & , & \frac{x^2}{2h^2} \end{array} \right] \\ \boldsymbol{N}^{II} & = & \left[\begin{array}{ccccc} \frac{x^2}{2h^2} - \frac{x}{h} + \frac{1}{2} & , & -\frac{x^2}{h^2} + \frac{x}{h} + \frac{1}{2} & , & \frac{x^2}{2h^2} \end{array} \right] \\ \boldsymbol{N}^{III} & = & \left[\begin{array}{ccccc} \frac{x^2}{2h^2} - \frac{x}{h} + \frac{1}{2} & , & -\frac{3x^2}{2h^2} + \frac{x}{h} + \frac{1}{2} & , & \frac{x^2}{h^2} \end{array} \right] \end{array} \tag{5.3}$$

5.2 Element stiffness matrices

Within each element of type J the strain $\epsilon(x)$ is calculated by

$$\epsilon(x) = \frac{dU(x)}{dx} = \frac{d}{dx} \boldsymbol{N}^J \boldsymbol{u} = \boldsymbol{B}^J \boldsymbol{u} \tag{5.4}$$

where $\boldsymbol{B}^J$ are the strain-displacement matrices (Eq. 3.3). Based on the recurrence relation there are special rules to get the derivative of a spline function. However, due to the concurrent formulation and purpose, the usual derivation as known for polynomials is also convenient and leads to

$$\begin{array}{rcl} \boldsymbol{B}^I & = & \left[\begin{array}{ccccc} \frac{2x}{h^2} - \frac{2}{h} & , & -\frac{3x}{h^2} + \frac{2}{h} & , & \frac{x}{h^2} \end{array} \right] \\ \boldsymbol{B}^{II} & = & \left[\begin{array}{ccccc} \frac{x}{h^2} - \frac{1}{h} & , & -\frac{2x^2}{h^2} + \frac{1}{h} & , & \frac{x}{h^2} \end{array} \right] \\ \boldsymbol{B}^{III} & = & \left[\begin{array}{ccccc} \frac{x}{h^2} - \frac{1}{h} & , & -\frac{3x}{h^2} + \frac{1}{h} & , & \frac{2x}{h^2} \end{array} \right] \end{array} \tag{5.5}$$

For building the element stiffness matrices the material matrix $\boldsymbol{C}$ is required. Here, in the one-dimensional case it is a scalar matrix $\boldsymbol{C} = [E]$ of Young's modulus E. The stress σ (Eq. 3.4) is calculated by

$$\sigma(x) = \boldsymbol{C}\boldsymbol{B}^J\boldsymbol{u} \tag{5.6}$$

For the segment basis length h and section area A the integral (Eq. 3.7)

$$\boldsymbol{K} = A\int_0^h \boldsymbol{B}^{\mathrm{T}}\boldsymbol{C}\boldsymbol{B}\,dx \tag{5.7}$$

leads to the following element stiffness matrices of type $J = I$, II and III.

$$\boldsymbol{K}^I = \tfrac{EA}{h}\begin{bmatrix} \frac{4}{3} & -1 & -\frac{1}{3} \\ -1 & 1 & 0 \\ -\frac{1}{3} & 0 & \frac{1}{3} \end{bmatrix} \quad \boldsymbol{K}^{II} = \tfrac{EA}{h}\begin{bmatrix} \frac{1}{3} & -\frac{1}{6} & -\frac{1}{6} \\ -\frac{1}{6} & \frac{1}{3} & -\frac{1}{6} \\ -\frac{1}{6} & -\frac{1}{6} & \frac{1}{3} \end{bmatrix} \quad \boldsymbol{K}^{III} = \tfrac{EA}{h}\begin{bmatrix} \frac{1}{3} & 0 & -\frac{1}{3} \\ 0 & 1 & -1 \\ -\frac{1}{3} & -1 & \frac{4}{3} \end{bmatrix} \tag{5.8}$$

5.3 Notes on global stiffness matrix

For a bar example the left boundary of the bar is modeled by element type I and the right boundary by element type III. All elements in between are of type II. It is important to note, that all shape functions of the B-Spline are not directly associated with nodal values or nodes. It is rather useful to regard a shape function as part of an element only. To establish the continuity of the displacement solution as required, it has to be ensured that the shape function segments of one B-Spline will be associated with the same global degree of freedom. In three neighboring elements (as in Fig. 5.2) the segment (c) of the left element, the segment (b) of the middle element and the segment (a) of the right element correspond to one and the same B-Spline shape function and need therefore to be associated to the same global degree of freedom.

5.4 Example: Homogeneous B-Spline bar elements of order k=2

The following example provides a clear and transparent access to the presented method of B-spline finite elements. It can be included into any introductory course on finite elements. Moreover, this example highlights some characteristics of B-spline finite elements and therefore prepares for further developments of these elements.

The stiffness matrix $\boldsymbol{K}$ of four B-Spline finite elements without consideration of displacement boundary conditions is composed of $\boldsymbol{K}^I$, $\boldsymbol{K}^{II}$ and $\boldsymbol{K}^{III}$ as

$$\boldsymbol{K} = \frac{EA}{h}\begin{bmatrix} \frac{4}{3} & -1 & -\frac{1}{3} & 0 & 0 & 0 \\ -1 & 1+\frac{1}{3} & -\frac{1}{6} & -\frac{1}{6} & 0 & 0 \\ -\frac{1}{3} & -\frac{1}{6} & \frac{1}{3}+\frac{1}{3}+\frac{1}{3} & -\frac{1}{6}-\frac{1}{6} & -\frac{1}{6} & 0 \\ 0 & -\frac{1}{6} & -\frac{1}{6}-\frac{1}{6} & \frac{1}{3}+\frac{1}{3}+\frac{1}{3} & -\frac{1}{6} & -\frac{1}{3} \\ 0 & 0 & -\frac{1}{6} & -\frac{1}{6} & \frac{1}{3}+1 & -1 \\ 0 & 0 & 0 & -\frac{1}{3} & -1 & \frac{4}{3} \end{bmatrix} \tag{5.9}$$

For best transparency of the method an academic example of simple system parameters without dimension is chosen. Length of the beam according to Fig. 5.3(a) is 4. Young's modulus E and area of section A are both set to 1, such that the factor $\frac{EA}{h} = 1$. The displacement boundary

Fig. 5.3: Static systems of a bar problem: (a) a bar loaded by F and (b) bar with constant line load p.

condition of the left end leads to elimination of first line and column of the matrix (Eq. 5.9) and therefore to

$$\boldsymbol{K} = \begin{bmatrix} \frac{4}{3} & -\frac{1}{6} & -\frac{1}{6} & 0 & 0 \\ -\frac{1}{6} & 1 & -\frac{1}{3} & -\frac{1}{6} & 0 \\ -\frac{1}{6} & -\frac{1}{3} & 1 & -\frac{1}{6} & -\frac{1}{3} \\ 0 & -\frac{1}{6} & -\frac{1}{6} & \frac{4}{3} & -1 \\ 0 & 0 & -\frac{1}{3} & -1 & \frac{4}{3} \end{bmatrix} \boldsymbol{u} = \begin{bmatrix} 0.5 \\ 1.5 \\ 2.5 \\ 3.5 \\ 4.0 \end{bmatrix} \boldsymbol{f} = \begin{bmatrix} 0 \\ 0 \\ 0 \\ 0 \\ 1 \end{bmatrix} \tag{5.10}$$

For system of Fig. 5.3(a) with the load $F = 1$ the load vector $\boldsymbol{f}$ is straightforward to construct. The solution of the equations system $\boldsymbol{K}\boldsymbol{u} = \boldsymbol{f}$ leads to $\boldsymbol{u}$ as provided above (Eq. 5.10). The composition of the linear displacement field by the B-spline shape functions according to this example is shown in Fig. 5.4.

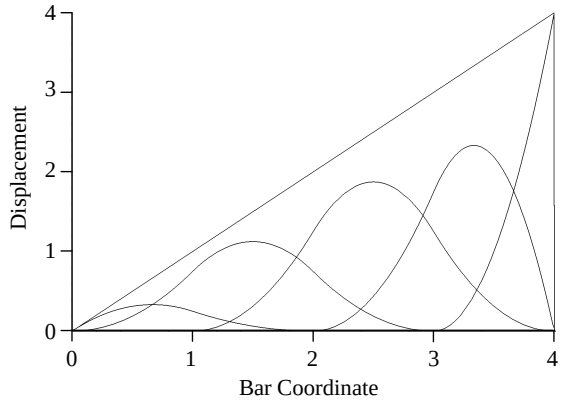

Fig. 5.4: B-Spline shape functions and displacement solution according to system in Fig. 5.3(a).

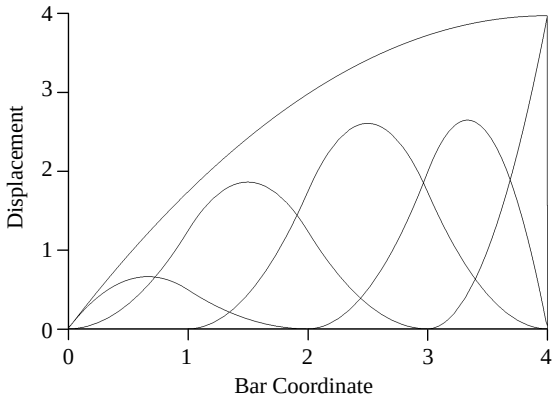

Fig. 5.5: B-Spline shape functions and displacement solution according to system in Fig. 5.3(b).

A further example with the same structural parameters and stiffness matrix with constant line load p as shown in Fig. 5.3(b) follows. The effective load associated to the segments of one element is the result of the integral (Eq. 3.8)

$$\boldsymbol{f} = \int_{x=0}^{h} \boldsymbol{N}^{\mathrm{T}} p(x) \mathrm{dx} \tag{5.11}$$

For a constant load of $p = 0.5$, the load function can be extracted from the integral, such that only the following integrals are relevant.

$$\begin{aligned} \textstyle\int_{x=0}^{h} \boldsymbol{N}^{I} \,\mathrm{dx} &= \begin{bmatrix} \frac{h}{3} & , & \frac{h}{2} & , & \frac{h}{6} \end{bmatrix} \\ \textstyle\int_{x=0}^{h} \boldsymbol{N}^{II} \,\mathrm{dx} &= \begin{bmatrix} \frac{h}{6} & , & \frac{2h}{3} & , & \frac{h}{6} \end{bmatrix} \\ \textstyle\int_{x=0}^{h} \boldsymbol{N}^{III} \,\mathrm{dx} &= \begin{bmatrix} \frac{h}{6} & , & \frac{h}{2} & , & \frac{h}{3} \end{bmatrix} \end{aligned} \tag{5.12}$$

Again, segments which belong to the same global degree of freedom are associated, such that the following load vector $\boldsymbol{f}$ and solution $\boldsymbol{u}$ to this problem is obtained.

$$\boldsymbol{f} = \begin{bmatrix} \frac{1}{3} & \frac{1}{2} & \frac{1}{2} & \frac{1}{3} & \frac{1}{6} \end{bmatrix}^{\mathrm{T}}, \qquad \boldsymbol{u} = \begin{bmatrix} 1.0 & 2.5 & 3.5 & 4.0 & 4.0 \end{bmatrix}^{\mathrm{T}} \tag{5.13}$$

As further explanation the first entry of $\boldsymbol{f}$ sums up from a segment b of type I and a segment a of type II, which is $\frac{1}{2} + \frac{1}{6} = \frac{2}{3}$ and multiplied by $p = 0.5$ results in $0.5\frac{2}{3} = \frac{1}{3}$. The displacement solution is graphed in Fig. 5.5. It corresponds to the exact analytical solution (Eq. 2.10), $EAU_{,xx} + p = 0$ with $U(x = 0) = 0$ and $\sigma(x = 4) = 0$, therewith $U = -\frac{1}{4}x^2 + 2x$.

6 TWO-DIMENSIONAL B-SPLINE FINITE ELEMENTS

6.1 Local interpolation scheme

The following method is formulated for orthogonal, two-dimensional meshes with uniform grid space h_x and h_y in x- and y-direction respectively. Initially, uniform, univariate B-splines of order k are generated. The required minimum size of the domain corresponds to $(2k - 1)$ grid intervals in both directions (Section 4.4). Subsequently, the uniform B-splines are scaled according to grid spaces h_x and h_y (Eq. 4.13). Bivariate B-splines result from the tensor product [10].

$$b^{j_x,j_y}(x, y) = b^{j_x}(x)\, b^{j_y}(y) \tag{6.1}$$

The superscripts j_x and j_y signify that various element types are used, such as in the one-dimensional case (Section 5.1). With respect to computational implementation it is not reasonable to explicitly build the bivariate B-splines in symbolic form, when it is sufficient to calculate discrete values of $b^{j_x,j_y}(x, y)$. Then, it is more efficient with respect to memory storage and number of operations to evaluate the factors $b^{j_x}(x)$ and $b^{j_y}(y)$, and apply these discrete values to Equation 6.1 to obtain $b^{j_x,j_y}(x, y)$. Bivariate B-splines as shape functions of two-dimensional finite elements are shown in Fig. 6.1.

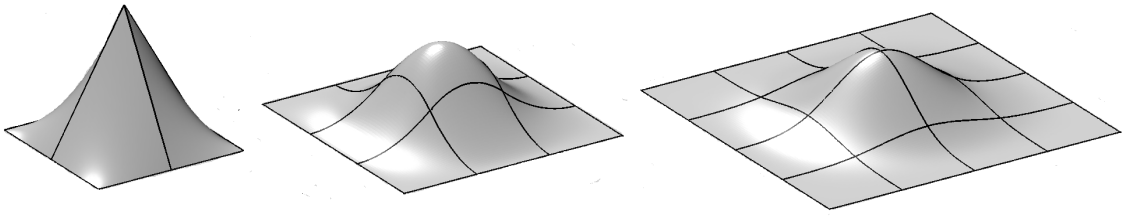

Fig. 6.1: Bivariate B-spline finite element shape functions: k=1, k=2 and k=3 (from left to right).

6.2 Element stiffness matrices

Similar to the one-dimensional case and as stated by the kinematics, derivatives of the shape functions $b^{j_x,j_y}(x, y)$ need to be computed. To obtain these partial derivatives at discrete coordinates it is convenient to reuse the principle of Equation 6.1 in the following form.

$$\frac{\partial b^{j_x,j_y}(x, y)}{\partial x} = \frac{\partial (b^{j_x}(x)\, b^{j_y}(y))}{\partial x} = \frac{\partial b^{j_x}(x)}{\partial x}\, b^{j_y}(y) \tag{6.2}$$

$$\frac{\partial b^{j_x,j_y}(x,y)}{\partial y} = \frac{\partial (b^{j_x}(x)\, b^{j_y}(y))}{\partial y} = b^{j_x}(x)\, \frac{\partial b^{j_y}(y)}{\partial y} \tag{6.3}$$

The interpolation matrices are created for individual elements which correspond to one grid patch. Analog to Equation 5.1 this is

$$\boldsymbol{U} = \boldsymbol{N}^{j_x,j_y} \boldsymbol{u} \tag{6.4}$$

for the two-dimensional case with

$$\boldsymbol{U} = \begin{bmatrix} U_x \\ U_y \end{bmatrix} \tag{6.5}$$

$$\boldsymbol{N}^{j_x,j_y} = \left[\begin{array}{ccc|ccc} N_1 & \dots & N_{\bar{n}} & & \mathbf{0} & \\ & \mathbf{0} & & N_1 & \dots & N_{\bar{n}} \end{array}\right]^{j_x,j_y} \tag{6.6}$$

$$\boldsymbol{u} = \begin{bmatrix} u_{x,1} & \dots & u_{x,\bar{n}} & u_{y,1} & \dots & u_{y,\bar{n}} \end{bmatrix}^{\mathrm{T}} \tag{6.7}$$

Here, the index $\bar{n}$ denotes the number of bivariate spline segments in one element which corresponds to $\bar{n} = (k+1)^2$ or if the order of B-splines is different in x- and y-direction $\bar{n} = (k_x+1)(k_y+1)$. The superscripts j_x and j_y define the element type in x- and y-direction, respectively. The strain-displacement relationship is

$$\boldsymbol{\epsilon} = \boldsymbol{B}^{j_x,j_y} \boldsymbol{u} \tag{6.8}$$

with the same degrees of freedom $\boldsymbol{u}$ (Eq. 6.7) and

$$\boldsymbol{\epsilon} = \begin{bmatrix} \epsilon_{xx} & \epsilon_{yy} & 2\epsilon_{xy} \end{bmatrix}^{\mathrm{T}} \tag{6.9}$$

$$\boldsymbol{B}^{j_x,j_y} = \left[\begin{array}{ccc|ccc} \frac{\partial N_1}{\partial x} & \dots & \frac{\partial N_{\bar{n}}}{\partial x} & & \mathbf{0} & \\ & \mathbf{0} & & \frac{\partial N_1}{\partial y} & \dots & \frac{\partial N_{\bar{n}}}{\partial y} \\ \frac{\partial N_1}{\partial y} & \dots & \frac{\partial N_{\bar{n}}}{\partial y} & \frac{\partial N_1}{\partial x} & \dots & \frac{\partial N_{\bar{n}}}{\partial x} \end{array}\right]^{j_x,j_y} \tag{6.10}$$

Recalling the constitutive law of plane stress (Eq. 2.9) yields the material matrix $\boldsymbol{C}$ as

$$\boldsymbol{C} = \frac{E}{1-\nu^2} \begin{bmatrix} 1 & \nu & 0 \\ \nu & 1 & 0 \\ 0 & 0 & \frac{1-\nu}{2} \end{bmatrix} \tag{6.11}$$

The stiffness matrices are evaluated by numerical integration

$$\boldsymbol{K}^{j_x,j_y} = t \frac{h_x}{2} \frac{h_y}{2} \sum_{i=1}^{n_x} \sum_{j=1}^{n_y} w_{x,i}\, w_{y,j} \left(\boldsymbol{B}^{j_x,j_y\,\mathrm{T}} \boldsymbol{C} \boldsymbol{B}^{j_x,j_y} \right) \tag{6.12}$$

where t is the depth of the two-dimensional system. It is practical to substitute $\boldsymbol{C}(E,\nu) = E\boldsymbol{C}(1,\nu)$ and to build the element stiffness matrices for Young's modulus $E = 1$. Then the stiffness matrix can be adapted to any Young's modulus by a simple scalar factor. The variables $w_{x,i}$ and $w_{y,j}$ denote the weighting factors of the numerical integration scheme as described in the following Section 6.3.

6.3 Gauss-Legendre numerical integration of variable order

For a limited number of integration points the coordinates and weights of the Gauss-Legendre numerical integration can be taken from tables as e.g. given by *Bathe* [1]. However, for a variable order k of B-spline finite elements it is required to implement the general scheme for a variable number of integration points. For a one-dimensional function $g(s)$ in the interval $[-1, 1]$ the fundamental equation is

$$\int_{-1}^{1} g(s)\, ds \approx \sum_{i=1}^{n} w_i\, g(s_i) \tag{6.13}$$

where w_i are the weights and s_i are the coordinates of the integration points. An integration of $g(x)$ in the interval $[x_a, x_b]$ can be replaced by an integration of $g(s)$ in the interval $[-1, 1]$

$$\int_{x_a}^{x_b} g(x)\, dx = \int_{-1}^{1} g(s)\, \det J\, ds \tag{6.14}$$

with the transformation of coordinates

$$x = \frac{1}{2}\left((x_b - x_a)\, s + x_a + x_b\right) \tag{6.15}$$

and the determinant of the Jacobian matrix

$$\det J = \frac{dx}{ds} = \frac{x_b - x_a}{2} \tag{6.16}$$

From Eqs. 6.13 to 6.16 it follows that a function $g(x)$ in an interval $[0, h]$ is numerically integrated as follows

$$\int_{0}^{h} g(x)\, dx \approx \frac{h}{2} \sum_{i=1}^{n} w_i\, g\left(\frac{h}{2}\,(1 + s_i)\right) \tag{6.17}$$

The coordinates of the integration points s_i correspond to the zero points of the Legendre polynomials in the interval $[-1; 1]$. The Legendre polynomials can be generated by the following recursion as documented in *Duschek* [3]

$$P_{n+1}(s) = \frac{2n+1}{n+1} s P_n(s) - \frac{n}{n+1} P_{n-1}(s) \tag{6.18}$$

where the Legendre Polynomials $P_0(s) = 1$ and $P_1(s) = s$ are used as start values. There is no closed-form solution to obtain the n zero points of $P_n(s)$, but the following lower and upper estimates of s_i are available.

$$-\cos\left(\frac{n - 0.5}{i + 0.5}\pi\right) < s_i < -\cos\left(\frac{n}{i + 0.5}\pi\right) \qquad \text{for} \quad i = 1, \ldots, n \tag{6.19}$$

There is always exactly one coordinate s_i in the intervals of Eq. 6.19. For the search of this zero point within a closed interval the bisection method is applied. As an alternative the more efficient, but apparently less stable Newton method shall be mentioned.

The weights w_i of the integration points s_i are determined by

$$w_i = \frac{2}{n P_{n-1}(s_i) \dfrac{dP_n(s_i)}{ds}} \tag{6.20}$$

The integration points are symmetric to the origin and the corresponding weighting factors are equal. Therefore the numerical effort can be reduced to one symmetric half. Clearly, for a odd number of integration points, one is located at the origin.

An application of the one-dimensional integration formula (Eq. 6.17) to the $x-$ and y-coordinate successively, transforms the symbolic integral for evaluating the element stiffness matrix (Eq. 3.7) into its numerical counterpart as given in Eq. 6.12. For B-spline shape functions of order k the integrands in Equation 6.12 will at maximum be a polynomial of order $2k$ with respect to either x or y. For the one-dimensional case n integration points exactly integrate a polynomial of at most order $(2n-1)$ such that in one dimension $n = k+1$ integration points would be required. In two dimensions this corresponds to an (unequally spaced) grid of $n \times n$ integration points.

6.4 Global formulation of B-spline finite element problem

A uniform, orthogonal, two-dimensional mesh of B-spline finite elements of variable order k is considered. The mesh includes $n_{ex} \times n_{ey}$ elements and $n_{nx} \times n_{ny}$ nodes. The global degrees of freedom are splitted[3] into x-and y-direction and the following numbering system refers to one direction only. Then, without activating displacement boundary conditions, there are $n_{sx} \times n_{sy}$ B-spline coefficients[4] assigned to the global mesh. The local degrees of freedom in one element correspond to $n_{cx} \times n_{cy}$ B-spline coefficients. For these definitions the following equalities hold

$$n_{nx} = n_{ex} + 1\,, \qquad n_{ny} = n_{ey} + 1\,, \tag{6.21}$$

$$n_{sx} = n_{ex} + k\,, \qquad n_{sy} = n_{ey} + k\,, \tag{6.22}$$

$$n_{cx} = k + 1\,, \qquad n_{cy} = k + 1\,, \tag{6.23}$$

The numbering of elements i_{eg}, nodes i_{ng}, global B-spline coefficients i_{sg} and local B-spline coefficients i_{cg} of an element can be defined as

$$i_{eg}(i,j) = i + j n_{ex} \quad \text{with} \quad i = 0 \ldots n_{ex} - 1, \quad j = 0 \ldots n_{ey} - 1, \tag{6.24}$$

$$i_{ng}(i,j) = i + j n_{nx} \quad \text{with} \quad i = 0 \ldots n_{nx} - 1, \quad j = 0 \ldots n_{ny} - 1, \tag{6.25}$$

$$i_{sg}(i,j) = i + j n_{sx} \quad \text{with} \quad i = 0 \ldots n_{sx} - 1, \quad j = 0 \ldots n_{sy} - 1, \tag{6.26}$$

$$i_{cg}(i,j) = i + j n_{cx} \quad \text{with} \quad i = 0 \ldots n_{cx} - 1, \quad j = 0 \ldots n_{cy} - 1, \tag{6.27}$$

where the universal variables i and j count the various entities in positive x- and y-direction, respectively. In adaption to the implementation the count variables start by 0. At the corners of element (i,j) there are the nodes (i,j), $(i+1,j)$, $(i+1,j+1)$ and $(i,j+1)$. Accordingly the local B-spline shape coefficients in element (i,j) refer to the global B-spline coefficients $(i \ldots i+k,\ j \ldots j+k)$. Therefore, the assignment of local B-spline coefficients (i^*, j^*) of an element (i,j) into the global vector of B-spline coefficients i_{sg} is defined as

$$i_{sg}(i,j,i^*,j^*) = (i + i^*) + (j + j^*) n_{sx} \tag{6.28}$$
$$\text{with } i = 0 \ldots n_{ex} - 1\,,\ j = 0 \ldots n_{ey} - 1\,,\ i^* = 0 \ldots k\,,\ j^* = 0 \ldots k$$

As for a one-dimensional example where e.g. $j = 0$ and $j^* = 0$ with $k = 2$ this means that segment $i^* = 2$ of element $i = 0$, segment $i^* = 1$ of element $i = 1$ and segment $i^* = 0$ of

[3] Similar as in the local degrees of freedom of Eq. 6.7

[4] In this context *B-spline coefficient* is used as illustrative synonym to *degree of freedom*.

element $i = 2$ are segments of one and the same B-spline $i_{sg} = 2$ (compare this to Section 5.3 and Fig. 5.2).

After the computation of all different element stiffness matrices, the assignment from local to global degrees of freedom as given by Eq. 6.28 provides a clear order to build the full singular global stiffness matrix. After that certain degrees of freedom need to be eliminated according to boundary conditions (Section 6.5).

However, one of the basic ideas of the present paper is not to store a global stiffness matrix. This possibility is supported by the uniformity of B-spline shape functions and the resulting low number of varying element stiffness matrices. A corresponding scheme of an iterative solver method is outlined in Section 6.6. Nevertheless the defined order of entities and the global ordering according to Eq. 6.28 is maintained.

6.5 Boundary conditions

With common finite elements boundary conditions are often treated in terms of nodal forces or nodal displacements only. In fact the underlying theory principally corresponds to that required for B-Spline finite elements. However, the characteristic of B-spline finite elements of order $k \geq 2$ that the values at nodes do not have a direct counterpart in the vector of unknowns require some more considerate treatment.

The required formulation to apply forces to the finite element system is already provided by Equation 3.8. Analog to the element displacement vector Eq. 6.7 the element vector of forces is

$$\boldsymbol{f} = \left[\begin{array}{ccc|ccc} f_{x,1} & \dots & f_{x,\bar{n}} & f_{y,1} & \dots & f_{y,\bar{n}} \end{array} \right]^{\mathrm{T}} \tag{6.29}$$

For the two-dimensional plane stress problem the vectors of body loads $\boldsymbol{p}_b$ and surface loads $\boldsymbol{p}_s$ are reduced by the dimension of depth and they are only functions of x and y.

$$\boldsymbol{p}_b = \begin{bmatrix} p_{bx} \\ p_{by} \end{bmatrix} \qquad \text{and} \qquad \boldsymbol{p}_s = \begin{bmatrix} p_{sx} \\ p_{sy} \end{bmatrix} \tag{6.30}$$

The integrals of Equation 3.8 are evaluated numerically as described in Section 6.3. The element forces can be assembled into the global vector of forces according to Section 6.4. The present implementation supports line forces along the edges of rectangular domains. With the modified B-splines towards the boundaries the definition of these loads principally corresponds to the one-dimensional case while still x- and y-direction need to distinguished.

Any polynomial load function $p_i(\xi)$ can be applied by defining a list of load terms $c_{i,j}\xi^j$, similar to Eq. 4.2, the result of which will be summed up. The variable ξ is representative for a local coordinate system. Furthermore it is noted that point forces at corner points can directly be added to the corresponding force vector entry as at the corners, as an exception, the relevant shape functions are equal to 1.

Therefore it is obvious that also displacement conditions on corner points can directly be defined. With the definition of Eq. 6.26 the corresponding degrees of freedom of the four corners are

$$i_{sg}(0,0)\,, \quad i_{sg}(n_{sx}-1,0)\,, \quad i_{sg}(0,n_{sy}-1)\,, \quad i_{sg}(n_{sx}-1,n_{sy}-1)\,, \tag{6.31}$$

As further possibility only displacement conditions along the edges of the domain are considered in the following. A constant displacement along an edge which equals to 0 is straightforward to define as the degree of freedom of shape functions which are unequal to 0 at this edge

needs to be set to 0. This is only possible through the introduction of the mentioned modified B-splines. The relevant degrees of freedom along the four edges are

$$i_{sg}(i,0)\,, \quad i_{sg}(n_{sx}-1,j)\,, \quad i_{sg}(i,n_{sy}-1)\,, \quad i_{sg}(0,j)\,, \tag{6.32}$$

with the range of i and j as in Eq. 6.26. Otherwise any polynomial displacement functions can be defined or approximated along the edges. This problem corresponds to the one-dimensional case. An equation system needs to be solved, where $n+k$ values of the predefined displacement function need to be evaluated to determine $n+k$ B-spline coefficients according to the definitions in Section 4.2. The $n+k$ function values are evaluated at equidistant coordinates along the edge in our approach. Other choices in the approximation of the displacement function are possible as described in Section 4.1. It is noted that also in this Section the applied numerical order referred to the full singular equation system as given in Eq. 3.12 such that the additional steps of Eq. 3.13 and Eq. 3.14 are required to solve for the unknowns.

6.6 Iterative solving of B-spline finite element problem without storage of global stiffness matrix

Grid-based modeling supports iterative solving of the equation system without storing a global stiffness matrix in the memory. Any data which is required from the global stiffness matrix, as e.g. a specific entry or row, can be reconstructed on basis of the element stiffness matrices. As an essential key this is efficient by a fast access to a low number of different element stiffness matrices. The predefined numbering system of Section 6.4 further reduces the required memory demand and number of operations in the algorithm in contrast to the topology of an arbitrary mesh. In summary only a few number of vectors need to be stored, as itemized in [5] for bilinear finite elements. Undoubtfully, at least, these are the global vector of displacements $\boldsymbol{u}$ and the global vector of $\boldsymbol{f}$. Some further auxiliary vectors are required which depends on the applied iterative solver method.

In the following such a matrix-free application of the conjugate gradient method, which originates from *Hestenes & Stiefel* [9], is briefly discussed. In its algorithm the global stiffness matrix $\boldsymbol{K}$ is only involved in the computation of the global matrix-vector product $\boldsymbol{K}\boldsymbol{v}$ where $\boldsymbol{v}$ is a global vector. From Eq. 3.10 it follows that this global matrix-vector product $\boldsymbol{K}\boldsymbol{v}$ can be replaced by a sum of element-based matrix-vector products $\bar{\boldsymbol{K}}^e\bar{\boldsymbol{v}}^e$ such as

$$\hat{\boldsymbol{v}} := \boldsymbol{K}\boldsymbol{v} = \sum_e \bar{\boldsymbol{K}}^e\bar{\boldsymbol{v}}^e \tag{6.33}$$

where $\bar{\boldsymbol{K}}^e$ and $\bar{\boldsymbol{v}}^e$ refer to the global ordering of degrees of freedom and $\hat{\boldsymbol{v}}$ only denotes the result vector. In practice it is only useful to store the element stiffness matrices according to the local degrees of freedom $\boldsymbol{K}^e$. Then the principle of Eq. 6.33 is represented by the following steps:

(1) Set all entries of $\hat{\boldsymbol{v}}$ to 0.
(2) Copy the adequate entries of $\boldsymbol{v}$ into $\boldsymbol{v}^e$.
(3) Perform local matrix vector product $\hat{\boldsymbol{v}}^e := \boldsymbol{K}^e\boldsymbol{v}^e$.
(4) Add $\hat{\boldsymbol{v}}^e$ to the adequate entries of the global vector $\hat{\boldsymbol{v}}$
(5) In a loop through all elements e continue by (2)

For ignoring global degrees of freedom with displacement boundary conditions, the corresponding entries within $\boldsymbol{v}$ and $\hat{\boldsymbol{v}}$ are simply set to zero. By this procedure the storage of a global stiffness matrix is superseded for B-spline finite elements of any order k.

This is also possible by the multigrid method which is much more efficient with respect to computation times. It is the ideal method for solving very large problems as the effort only increases linear with problem size. However, in this paper the multigrid method is out of scope. It shall only be mentioned that *Höllig [11]* presented the multigrid method for web-splines where such B-splines finite elements are defined on all grids. As an alternative it can be useful to implement B-splines finite elements into an existing multigrid environment [5, 8] with classical finite elements by only creating adequate mutual transfer operators between a mesh of B-splines finite elements and a mesh of classical finite elements.

6.7 Example: Homogenous two-dimensional problem

In this example, the approximation quality of B-spline finite elements is evaluated with respect to variable order of B-splines (p-version) and variable size of elements (h-version). Therefore the example is sufficiently complex and the analytical solution is known such that the error analysis is accurate. The analytical solution of this example is

$$F = \text{Re}\left((x+iy)^{\eta}\right) \tag{6.34}$$

where F is the Airy function [15], i is the imaginary unit $i^2 = -1$ and Re means the real part of a complex number. Any valid solution to Airy's function F follows the condition $\Delta\Delta F = 0$. The stresses are defined as

$$\sigma_{xx} = F_{,yy} \ , \qquad \sigma_{yy} = F_{,xx} \ , \qquad \sigma_{xy} = -F_{,xy} \tag{6.35}$$

These stresses are applied as boundary conditions in terms of load p_x and p_y to the system shown in Fig. 6.2.

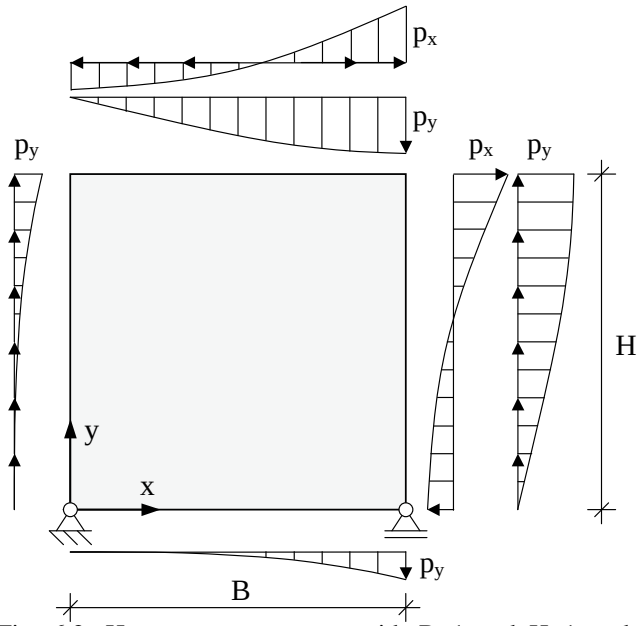

Fig. 6.2: Homogeneous system with B=1 and H=1 under higher-order polynomial loads p_x and p_y along its boundaries.

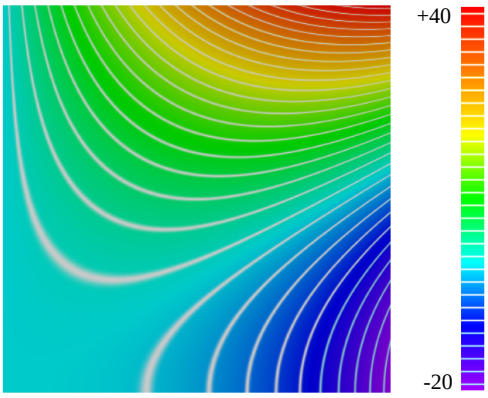

Fig. 6.3: B-spline finite element solution of stress σ_{xx} to problem of Fig. 6.2 for $k = 4$.

The load functions shown in Fig. 6.2 qualitatively correspond to Equation 6.34 with $\eta = 5$ which is $F_{\eta=5} = x^5 + 10x^3y^2 + 5xy^4$. For $\eta = 5$ the analytical stress solution is

$$\sigma_{xx} = -20x^3 + 60xy^2 \ , \qquad \sigma_{yy} = 20x^3 - 60xy^2 \ , \qquad \sigma_{xy} = 60x^2y - 20y^3 \tag{6.36}$$

For the boundaries where $x = 0$, $y = 0$, $x = 1$ and $y = 1$ it is straightforward to define the tractions p_x and p_y from these stresses. The inner potential energy Π_i of the system is defined as

$$\Pi_i = \frac{1}{2} \int_{x=0}^{1} \int_{y=0}^{1} \boldsymbol{\sigma}^{\mathrm{T}} \boldsymbol{\epsilon} \, \mathrm{dx} \, \mathrm{dy} \tag{6.37}$$

For $\eta = 5$ the inner potential is $\Pi_i(\eta = 5) = 329\frac{1}{7}$. The inner potential of the finite element solution will be less, or equal in case it corresponds to the analytical solution. The relative error of the inner potential of the finite element solution to the analytical solution is a reference value for the accuracy of the finite elements. In Figs. 6.4 and 6.5 this error is labeled as relative error in energy. These diagrams show the convergence of this error with respect to order of B-splines k (Fig. 6.4) and element size h (Fig. 6.5).

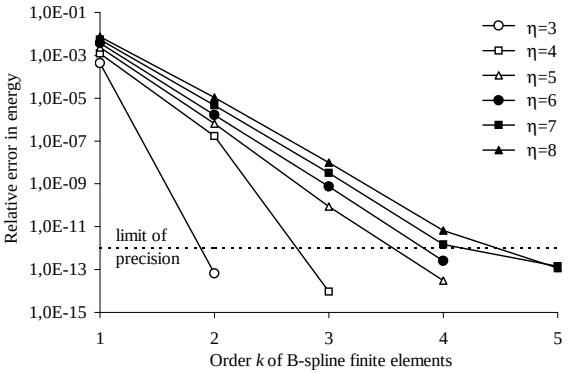

Fig. 6.4: Convergence of error with respect to polynomial order k for a constant size of elements $h = \frac{8}{128}$.

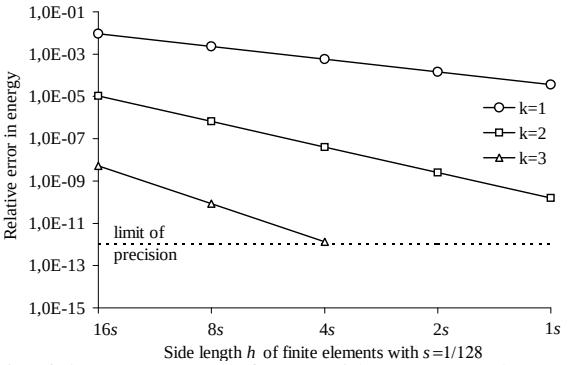

Fig. 6.5: Convergence of error with respect to element size h for the example $\eta = 5$.

It follows from these diagrams that it is much more efficient to decrease the error by an increase of polynomial order k than by an increase of element number (or equivalent decrease of element size). It is a well known fact that the p-version is better for homogeneous problems than the h-version. This example shows that implementation of the proposed B-splines finite elements and the routine of definined higher-order polynomial load function is accurate. A limit of tolerance due to limited computational precision is carefully assigned to the dimension 10^{-12} of relative error in energy. Values below practically correspond to the exact solution. As for example for $\eta = 5$ the stress functions are at maximum of polynomial order 3, then the corresponding displacement function is at maximum of order 4. Therefore B-spline finite elements of the order $k = 4$ shall lead to the exact solution which is shown to be true in Fig. 6.4 (within the tolerance of precision). Fig. 6.3 illustrates the corresponding solution of stress σ_{xx}.

According to *Zienkiewicz & Taylor* [19] some error convergence rate estimators are briefly outlined. Assuming that the exact displacement solution can be approximated by a Taylor serie, the displacement solution of the finite elements only include terms up to the order k. Then, the error only includes terms of the order $k + 1$ or higher. Therefore this error is estimated to converge by the order $O(h^{k+1})$. The strains are the first derivatives of the displacements such that the error in strains is assigned to one order below $O(h^k)$. Accordingly, an estimate of the

Error(2h) / Error(h)					
	a priori	$h = 8s$	$h = 4s$	$h = 2s$	$h = 1s$
$k = 1$	4	3.9904	3.9973	3.9992	3.9998
$k = 2$	16	16.043	16.012	16.003	16.003
$k = 3$	64	60.710	63.577	-	-

Table 1: Convergence rates with respect to the results presented in Fig. 6.5.

convergence rate of the inner potential Π_i (Equation 6.37) leads to the order $O(h^{2k})$. For the example in Fig. 6.5, the convergence rate estimator is $O(h^2)$ for $k = 1$, $O(h^4)$ for $k = 2$ and $O(h^6)$ for $k = 3$, which fits quite well to the achieved results as illustrated in Table 1. Therefore without proof the results indicate that the convergence rate estimator is also applicable to B-spline finite elements of variable order k.

7 MULTIPHASE FINITE ELEMENT CONCEPT FOR HETEROGENEOUS SOLIDS

7.1 Original mechanical problem with material discontinuity and substitute problem with continuous material function

The multiphase finite element concept is introduced for the mechanical analysis of heterogeneous solids. Before evaluating the corresponding finite element formulation, it is useful to show the main characteristics of the fundamental mechanical theory with respect to heterogeneous materials. Furthermore the original mechanical problem of heterogeneous material will be substituted by a transformed problem which will also converge to the exact solution while it initially appears less effective. However, it will be shown that this transformation cures a severe defect of the multiphase finite element solution, while the induced error by the substitute problem is comparatively low.

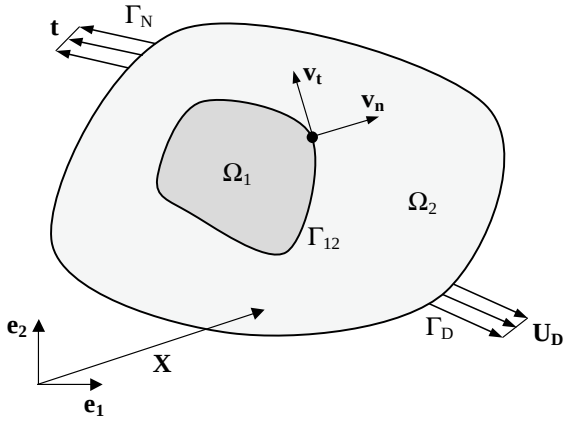

Fig. 7.1: Original problem with material discontinuity

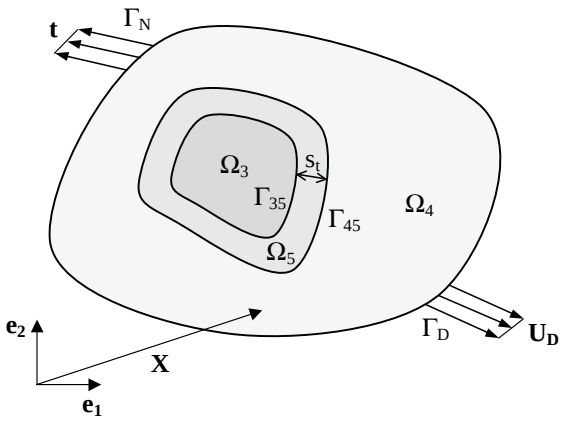

Fig. 7.2: Substitute problem with continuous material

As a principle example of a heterogeneous material, in Fig. 7.1 an inclusion (Ω_1) in a matrix material (Ω_2) is shown. Without the inclusion, the illustrated problem corresponds to the boundary value problem of linear elasticity as stated in Section 2. Additional compatibility conditions can be formulated for the rigid bonded interface between Ω_1 and Ω_2 which is denoted as Γ_{12}. Rigid bond is expressed by $\boldsymbol{U}^1 = \boldsymbol{U}^2$ on Γ_{12} where the superscript i refers to the domain Ω_i.

In terms of stresses and strains, the compatibility conditions are

$$\sigma^1_{nn} = \sigma^2_{nn} \ , \qquad \sigma^1_{nt} = \sigma^2_{nt} \ , \qquad \epsilon^1_{tt} = \epsilon^2_{tt} \ , \qquad \text{on } \Gamma_{12} \tag{7.1}$$

where the indices n and t correspond to the normal and tangential directions of the interface, $\boldsymbol{v}_n$ and $\boldsymbol{v}_t$ on Γ_{12}, as sketched in Fig. 7.1. Invoking the plane stress material law leads to

$$\epsilon^i_{nn} = \frac{1-\nu_i^2}{E_i}\sigma_{nn} - \nu_i \epsilon_{tt} \tag{7.2}$$

$$\sigma^i_{tt} = \nu_i \sigma_{nn} + E_i \epsilon_{tt} \tag{7.3}$$

$$\epsilon^i_{nt} = \frac{1+\nu_i}{E_i}\sigma_{nt} \tag{7.4}$$

which highlights that apart from some possible exceptions for different materials the following inequalities may occur

$$\epsilon^1_{nn} \neq \epsilon^2_{nn} \ , \qquad \epsilon^1_{nt} \neq \epsilon^2_{nt} \ , \qquad \sigma^1_{tt} \neq \sigma^2_{tt} \ , \qquad \text{on } \Gamma_{12} \tag{7.5}$$

For the subsequent approach it is especially important to note that some strains will not be continuous at a material discontinuity. However, the B-spline basis of the introduced finite elements for a polynomial order of $k \geq 2$ is always continuous in its derivatives and therefore only enables continuous strain fields. This discrepancy of continuity or discontinuity as described would lead to a severe defect if the B-Spline finite element method is applied to the original problem (Fig. 7.1).

Instead, a transformed problem is introduced (Fig. 7.2). The discontinuous material field is approximated by a smooth, continuous material field. The following conditions are introduced.

$$\Omega_3 \subset \Omega_1 \ , \qquad \Omega_4 \subset \Omega_2 \ , \tag{7.6}$$

with

$$E_3 = E_1 \ , \qquad E_4 = E_2 \ , \qquad \nu_3 = \nu_1 \ , \qquad \nu_4 = \nu_2 \ , \tag{7.7}$$

The material in Ω_5 is defined such that

$$E_5(\boldsymbol{X}) = E_3 \quad \text{and} \quad \nu_5(\boldsymbol{X}) = \nu_3 \qquad \text{on } \Gamma_{35} \tag{7.8}$$

$$E_5(\boldsymbol{X}) = E_4 \quad \text{and} \quad \nu_5(\boldsymbol{X}) = \nu_4 \qquad \text{on } \Gamma_{45} \tag{7.9}$$

The defined material transition in Ω_5, as well as its boundaries Γ_{35} and Γ_{45}, is assumed to be sufficiently smooth. The material transition in Ω_5 is monotonic in a section perpendicular to Γ_{35} or Γ_{45}. Then, with the definition that

$$s_t \longrightarrow 0 \tag{7.10}$$

which corresponds to

$$\Omega_3 \longrightarrow \Omega_1 \ , \qquad \Omega_4 \longrightarrow \Omega_2 \ , \tag{7.11}$$

a continuous substitute problem is generated which will converge to the original problem and therefore to the exact solution. However, for finite values of s_t, the width of the transition zone Ω_5 (Fig. 7.2), all strains and stresses will be continuous in the substitute problem. The B-spline finite elements can well be applied to the substitute problem, as B-spline finite elements are effective in the approximation of smooth solutions.

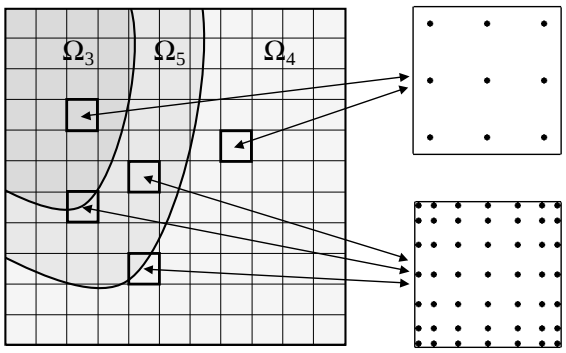

Fig. 7.3: Adapted number of integration points in multiphase finite elements.

7.2 Description of multiphase finite elements

Finite element meshes which are aligned to phase boundaries are the conventional way to analyze heterogeneous materials. But aligned mesh generation can become very complex, especially with regard to irregular shapes and three-dimensional models. Alternatively, an unaligned projection on a grid of conventional finite elements is demonstrated in [5]. It is possible to refine the discretization of the mesoscale geometry by multiphase finite elements [18, 21, 20] without increasing the number of elements or degrees of freedom.

In the preparation of an element stiffness matrix for each integration point i the integrands $\bar{\boldsymbol{K}}_i^e$ will initially be prepared and stored for a Young's modulus $E = 1$ in matrix $\boldsymbol{C}$ (Eq. 6.12). Based on these parts $\bar{\boldsymbol{K}}_i^e$ the assembly of specific element stiffness matrices e with different Young's modulus in each integration point $(E_1^e \dots E_n^e)$ is very fast established by

$$\boldsymbol{K}^e(E_1^e \dots E_n^e) = \sum_{i=1}^{n} E_i^e \, \bar{\boldsymbol{K}}_i^e \tag{7.12}$$

where in comparison to Eq. 6.12 the the two sums have been reduced to one sum over $i = 1 \dots n$ with $n = n_x n_y$. For finite elements of homogeneous material the order of the integrand only depends on the order of B-splines k (Eq. 6.12). With both, the shape functions and material function, being polynomials, a higher number of integration points can be determined such that the integration will be exact (Section 6.3). Otherwise, if an element crosses an interface a higher number of integration points generally increases the integration accuracy. Fig. 7.3 illustrates the idea of an adapted various number of integration points according to the material defined within the finite element.

It is pointed out that the evaluation of $\boldsymbol{K}^e$ as in Eq. 7.12 will increase the effort within the conjugate gradient method with respect to Eq. 6.33, but only for heterogeneous elements. The number of degrees of freedom does not increase.

By the combination of the multiphase concept and B-spline elements, the geometrical resolution and the approximation quality of each finite element can be controlled based on an efficient local formulation. It is pointed out that only in combination with smoothing of the material function as defined by the substitute problem (Section 7.1) smooth stress solutions can be achieved. Otherwise, also with classical finite elements the multiphase concept leads to defective jumps in tractions along an material interface. Subsequently, some examples are introduced to test the proposed method in the Sections 7.3 to 7.6 and a final discussion of the overall error is found in Section 7.7.

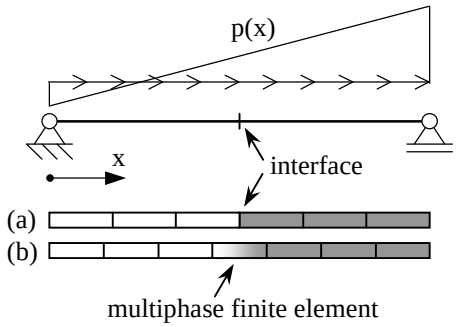

Fig. 7.4: Bar system with material discontinuity and finite element discretizations

7.3 Example: one-dimensional multiphase B-spline finite elements

A one-dimensional example of a bar with material discontinuity is presented. The system corresponds to that of Fig. 7.4. The load function is $p(x) = \frac{1}{40}x - 0.5$. The length of the bar is 100 cm. Section area is constant at 5 cm^2. A material discontinuity is located at the center of the bar at $x = 50$ cm. The Young's modulus of the left half ($0 \leq x < 50$ cm) is $E_1 = 3000\frac{\text{kN}}{\text{cm}^2}$ and that of the right half ($50 < x \leq 100$ cm) is $E_2 = 6000\frac{\text{kN}}{\text{cm}^2}$. The problem is analyzed by B-spline finite elements of order $k = 2$ in two variants. In the first example the bar is modeled by six B-spline finite elements. Three left of the material discontinuity obtain the parameter E_1 and three of the right parameter E_2 (Fig. 7.4(a)). In the second example the bar is modeled by seven finite elements (Fig. 7.4(b)). The three left most and right most B-spline finite elements are assigned to the parameters E_1 and E_2, respectively. In the center there is a multiphase B-spline finite element based on a linear material transition function from E_1 to E_2. The results of this example are shown in Fig. 7.5. In the variant of the multiphase element, it is visible that the stress solution is continuous and less deviating from the exact solution. Here, the exact solutions correspond to the original problem (Fig. 7.5, left) and to the transformed problem (Fig. 7.5, right).

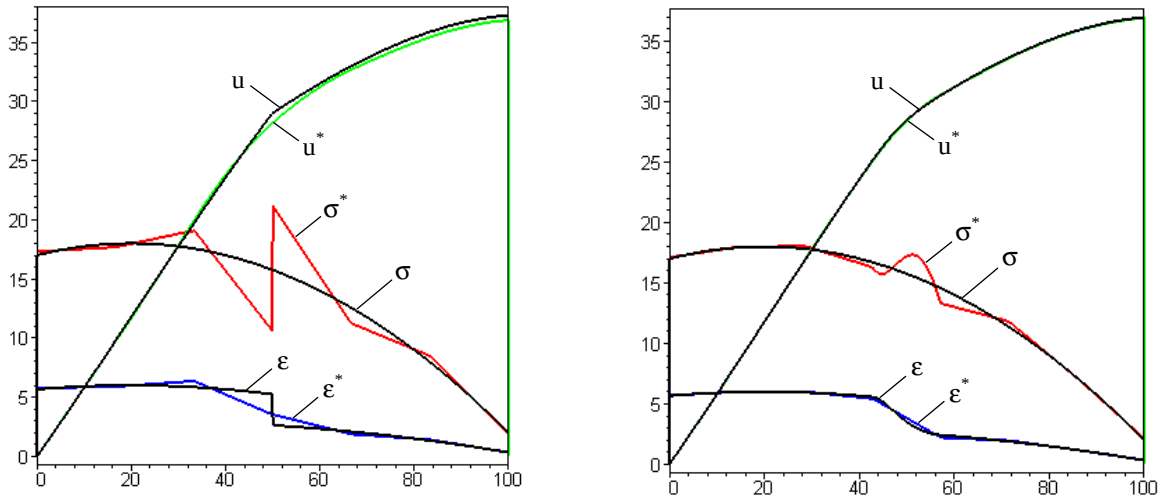

Fig. 7.5: Analytical solutions and finite element solutions, marked by *, for B-spline finite elements (left) and multiphase B-spline finite elements (right) for a loaded one-dimensional tension bar with material discontinuity (left) and linear material transition within one finite element (right) in terms of displacement u (magnified by factor 100), strain ϵ (magnified by factor 1000) and stress σ.

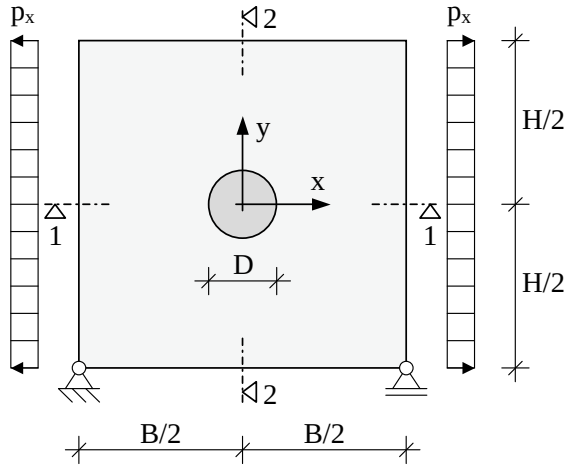

Fig. 7.6: Two-dimensional solid with circular inclusion under uniaxial stress p_x=10 (B=H=128, D=8).

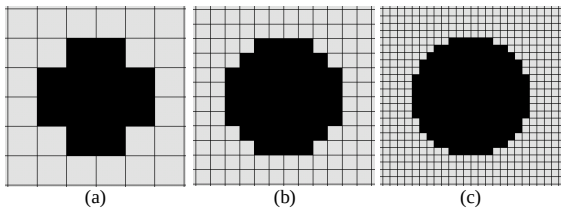

Fig. 7.7: Pixel models labeled as (a) Model 1, (b) Model 2 and (c) Model 3.

7.4 Example: Elastic circular inclusion in a matrix based on plain grid discretization

According to the provided theory on multiphase finite elements, an example of an elastic circular inclusion is introduced (Fig. 7.6). The inclusion and the matrix material are isotropic. The Young's modulus of the matrix is $E_{\text{matrix}} = 100000$ and of the inclusion is $E_{\text{inclusion}} = 200000$. The Poisson's ratio of both materials is $\nu_{\text{matrix}} = \nu_{\text{inclusion}} = 0.2$. The images of various grid discretizations of the spherical inclusions are shown in Fig. 7.7. The continuous material field, namely in the Young's modulus, is achieved by simple averaging of nodal values as illustrated in Figs. 7.8 and 7.9.

This example provides a basic study of the proposed method with respect to the mechanical analysis of materials with several inclusions as e.g. in concrete or other comparable heterogeneous solids. It is well suitable as the analytical solution for a circular inclusion in an infinite plate is available. It originates from *Muskhelishvili, 1952,* and is documented in [12]. In this example a ratio $16:1$ of plate dimension (B, H, in Fig. 7.6) to the diameter of the inclusion (D in Fig. 7.6) is assumed to be an acceptable approximation to which the analytical solution fits. It is therefore regarded as reference solution to this example. Here, it shall only be noted that analytically the stress state within the inclusion is constant, e.g. for this example the stresses are $\sigma_{xx} = \frac{825}{68} \approx 12.132$ and $\sigma_{yy} = \frac{25}{68} \approx 0.3676$. The analytical solution of stress σ_{xx} is shown in Fig. 7.11. The finite element solution of Model 2 with usual bilinear finite elements or, equivalent, B-spline finite elements of order $k = 1$ is shown in Fig. 7.10. In its comparison to the analytical solution it is visible by the naked eye that this finite element solution is

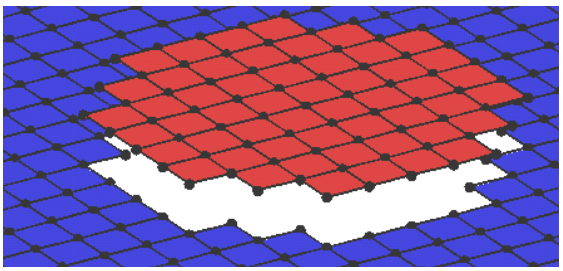

Fig. 7.8: Isometric view on Young's modulus of two-dim. solid with grid discretization of circular inclusion

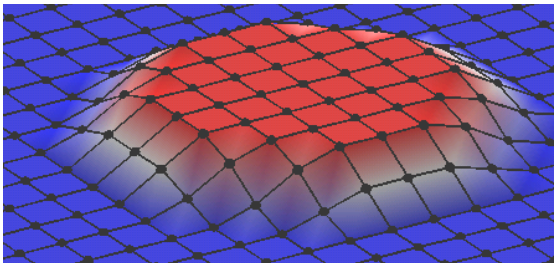

Fig. 7.9: Continuous Young's modulus by averaging of nodal values shown in Fig. 7.8

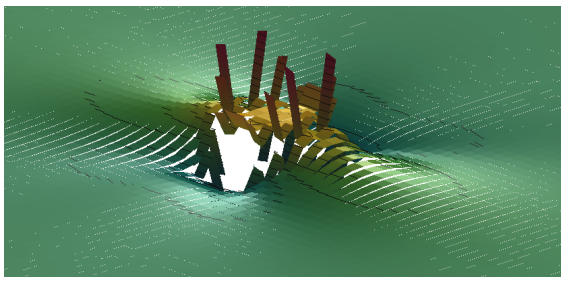

Fig. 7.10: Stress σ_{xx} of model in Fig. 7.8 by classical bilinear finite elements

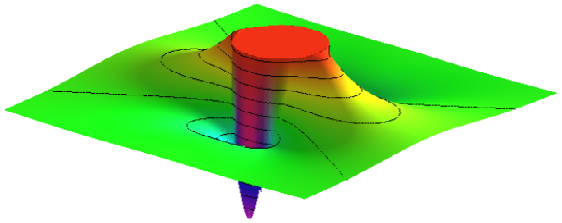

Fig. 7.11: Analytical solution of stress σ_{xx} for system of circular inclusion (Fig. 7.6)

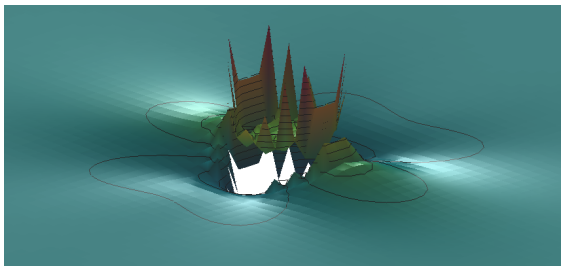

Fig. 7.12: Stress σ_{xx} of model in Fig. 7.8 by B-spline finite elements of order k=2

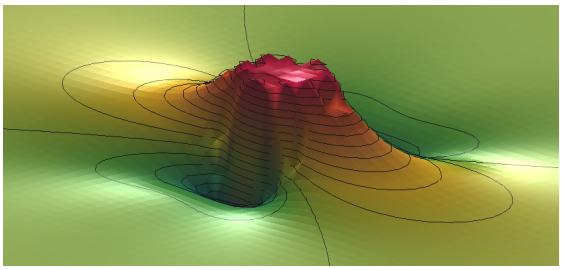

Fig. 7.13: Stress σ_{xx} of model in Fig. 7.9 by multiphase B-spline finite elements of order k=2

severely defective along the grid-based material interface approximation. The same effect is observed for B-spline finite elements of order $k = 2$ (Fig. 7.12). However, the application of multiphase B-spline finite elements of order $k = 2$ in combination with the transformed model of Fig. 7.9 leads to an essentially improved solution[5] (Fig. 7.13). As expected the solution of stress is continuous according to the theory of the substitute problem (Section 7.1).

For a qualitative comparison of the discretization by multiphase B-spline finite elements of order $k = 2$ to the analytical solution with respect to variable resolution (Model 1 to 3) two sections are selected as illustrated in Fig. 7.6, labeled as sections 1-1 and 2-2. All Figs. 7.14 to 7.17 show that principally the correct dimension in the stresses is matched[6].

From Model 1 to Model 3 a slight improvement in accuracy can be seen in stress σ_{xx} of Fig. 7.14. The evaluation of stress σ_{xx} of Fig. 7.15 is less clear. On one hand there is an improvement in accuracy with respect to the minimum and on the other hand inaccuracies develop at the edges of the center plane. A clear conclusion can not be drawn about the improvement of quality from Model 1 to Model 3.

Fig. 7.16 shows that with increasing resolution the peaks in stress σ_{yy} are approximated better. However, the development of stress σ_{yy} in Fig. 7.17 with increasing resolution of the model is more difficult to interpret. There are parts of improved and worse approximation.

Nevertheless, the major conclusion of this example is that principally the multiphase finite elements in combination with the transformed problem lead to reasonable results. This is a relevant improvement with respect to plain grid discretization where the stresses are severely defective. Therefore this example presents that the basic idea works in principle. But the considered variants did not lead to a clear conclusion how these models can further be improved. Therefore this aspect will be highlighted in further examples.

[5]It is noted that for this diagram only the stress in the corners of the elements are evaluated. A more detailed evaluation will be shown in the next example.

[6]Only values at the corners of the elements are evaluated and interconnected linear.

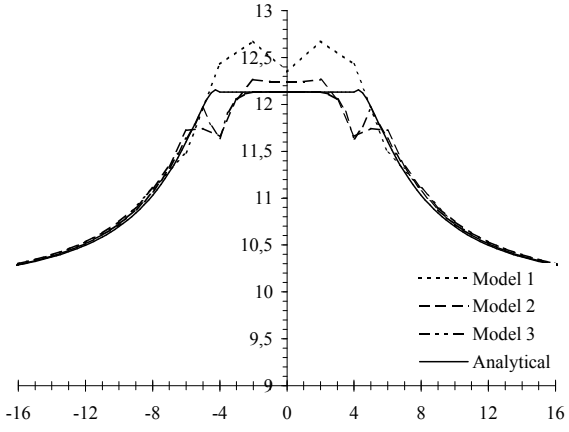

Fig. 7.14: Stress σ_{xx} of section 1-1

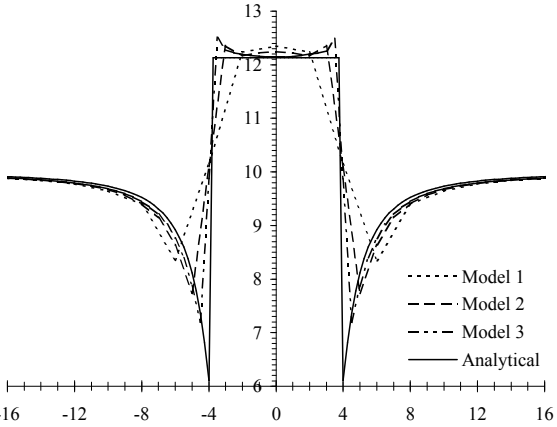

Fig. 7.15: Stress σ_{xx} of section 2-2

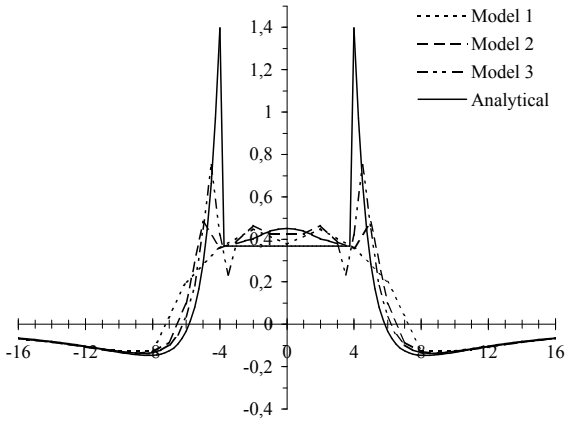

Fig. 7.16: Stress σ_{yy} of section 1-1

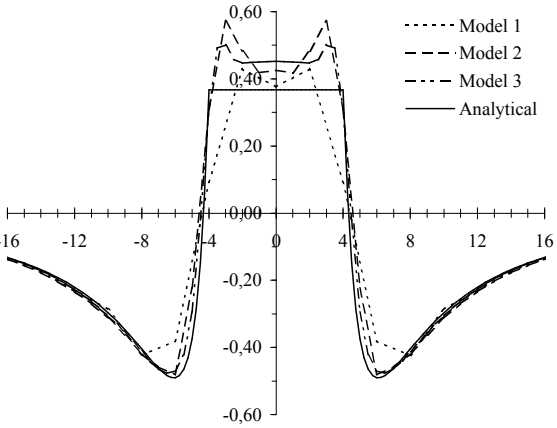

Fig. 7.17: Stress σ_{yy} of section 2-2

7.5 Example: Elastic spherical inclusion in a matrix based on mapping of geometry

This example is mostly identical to the prior example. The only, but essential difference is the effective description of the circle on the finite element mesh. In the foregoing example, first a plain grid discretization was generated where one finite element either belongs to the inclusion or to the matrix (Fig. 7.8). Then the material model was smoothed by averaging of nodal values (Fig. 7.9). The isolines which correspond to Model 2 (Fig. 7.9) are shown in Fig. 7.18(a). As an improved option the circular inclusion and a circular transition function (compare to Ω_5) are

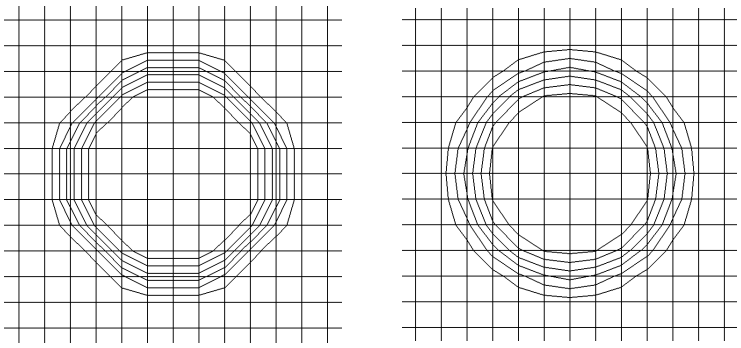

Fig. 7.18: Isolines of material transition function of (a) model in Fig.7.9, (b) based on mapping of material function on element centers with subsequent interpolation at nodes.

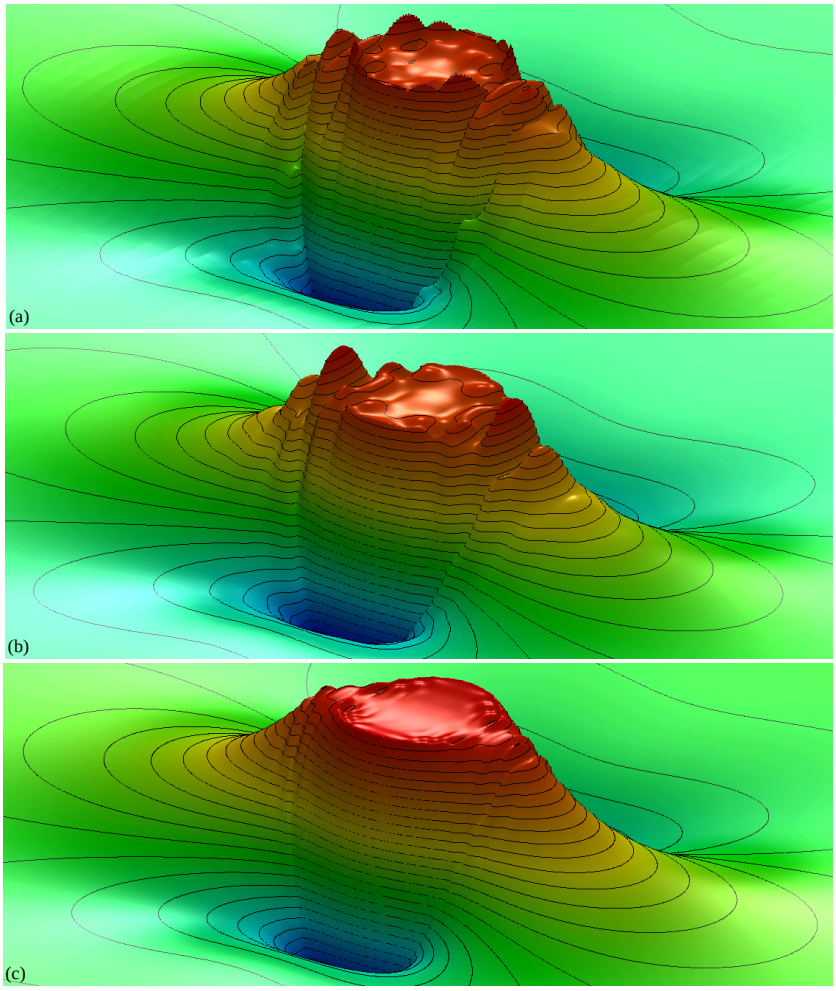

Fig. 7.19: Stress σ_{xx}, multiphase B-spline finite elements of order (a) $k = 2$, (b) $k = 3$ and (c) $k = 3$, finer mesh.

mapped onto the centers of the elements, first. Then, the material properties of the nodes are computed as the averages of the neighboring element centers. This leads to a quite improved topology of material properties (Fig. 7.18(b)). It is interesting to note that this indirect method apparently leads to a more accurate geometrical representation than the direct mapping on the nodes with subsequent bilinear averaging within the finite elements (without illustration).

However, it is clear that some geometrical error is induced by any of these procedures which needs to be distinguished from the inherent approximation quality of multiphase B-spline finite elements. Therefore in this example the circle and the transition function are exactly mapped onto the integration points of the finite elements. This is only possible if an analytical description of the inclusion is available such as in this case of a circle. However, for other inclusion shapes such analytical functions are available as well [5]. The number of integration points is increased by 2 with respect to one dimension to cover the heterogeneous material within the finite element.

The basic aspect of this example is to analyze if an increase of element number (h-method) or element order k (p-method) leads to improved results and shows clear convergence. Figure 7.19(a) shows the solution of stress σ_{xx} for multiphase B-splines of order $k = 2$. In Figure 7.19(b) the order of the elements is $k = 3$. With a C^2-continuous material transition function and C^2-continuous B-spline finite elements this stress solution is not only C^0-, but C^1-continuous (in contrast to Fig. 7.19(a)). It appears smoother, but some defective oscillations

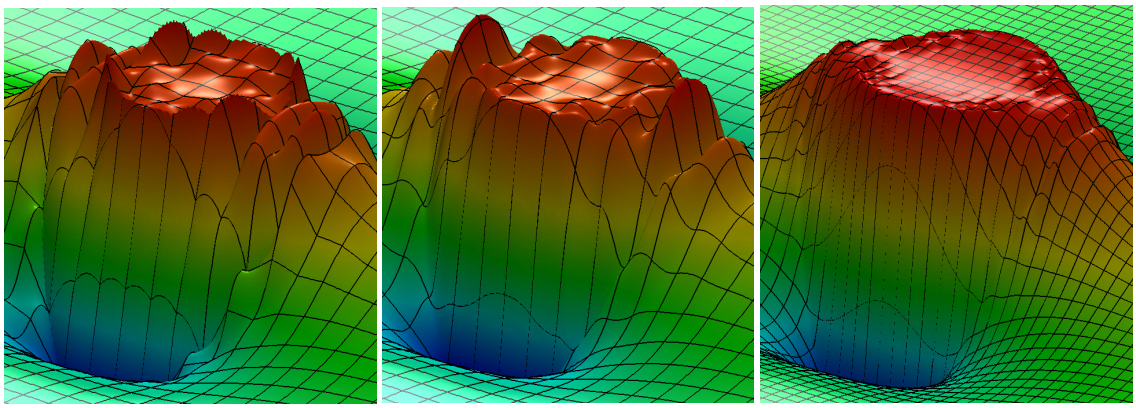

Fig. 7.20: Stress σ_{xx} as in Fig. 7.19, but magnified and with element grid (a to c correspond).

are obvious. Halving the mesh size leads to the result of Fig. 7.19(c).

Qualitatively, this result is essentially improved. The increase of order k had less visible effect. Therefore it is supposed that the h-version is more effective than the p-version for the heterogenous case (in contrast to the homogeneous case, Section 6.7). As the major conclusion of this example, it is noted that multiphase B-spline finite elements offer a reasonable alternative in modeling heterogeneous materials. The required element number appears reasonable too. The element resolution of Fig. 7.19 is shown in Fig. 7.20. For an effective use and best knowledge of this method further studies are performed.

7.6 Example: Uniaxial stress case of one material transition

The focus of this example is the exact analysis of the defect in the stress solution for one material transition according to Figure 7.21. It is a one-dimensional example but was computed by the two-dimensional implementation. The Poisson's ratio is set to zero for both materials. The parameter study includes a variation of material transition functions as is shown in Fig. 7.22. The linear function only generates a C^0-continuous transition. The continuity which results from the cubic function is C^1 and that of the quintic function is C^2. The material functions will

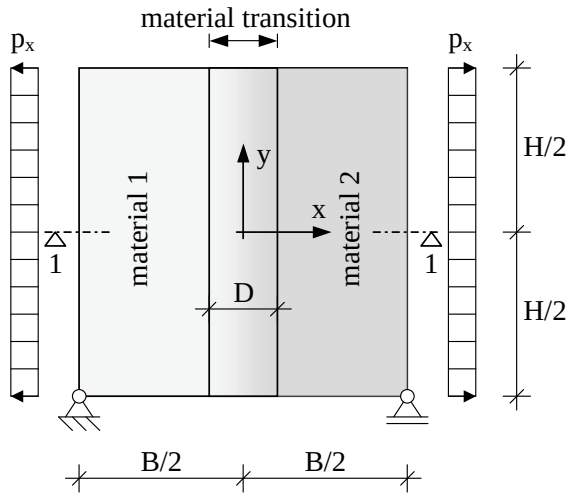

Fig. 7.21: Two-dimensional solid with one material transition zone, $p_x = 1\frac{\mathrm{N}}{\mathrm{mm}^2}$, B=H=128mm, D=16mm.

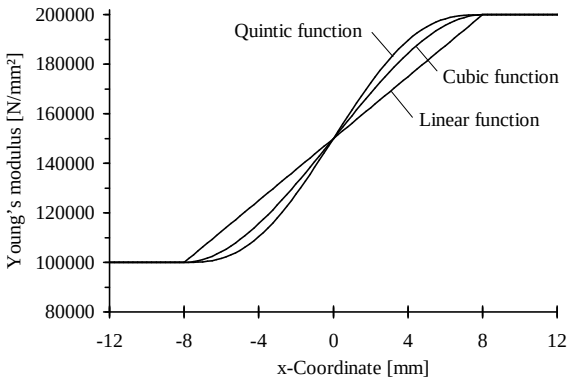

Fig. 7.22: Various material transition functions for the system of Fig. 7.21

be directly mapped onto the integration points of the finite elements. Furthermore a variation of element number and variation of element order k is examined. The finite element results will be analyzed in terms of error in stress and error in energy in comparison to the exact analytical solution.

The exact solution to this problem is $\sigma_{xx} = 1\frac{\mathrm{N}}{\mathrm{mm}^2}$ in the whole domain. Figs. 7.23 to 7.25 show the multiphase B-spline finite element solutions for a linear transition, a cubic transition and a quintic transition, respectively. Here, element size is constant $h = 4$mm. The varying parameter is the order k of applied B-spline shape functions. Figure 7.23 shows a comparatively good solution for $k = 2$ and a change for the worse for $k = 3$. This can be explained as B-splines of order $k = 3$ are C^2-continuous while due to the linear transition function the exact solution to this problem in terms of displacement is only C^1-continuous. This leads to the significant peaks in the solution at the x-coordinates $x = -8$ and $x = 8$. Further increase of B-spline order k does not cure this defect. Figure 7.24 shows a better solution in stress for $k = 3$ than for $k = 2$. The foregoing effect only occurs for $k = 4$, but is less severe. Again, a further increase of order k does not lead to convergence.

Figure 7.25 is only included to find out if a further increase of continuity in the material transition function would essentially increase the possible approximation quality with respect to an increase of k. In fact, then a relative good solution is achieved for $k = 5$, but the effect does

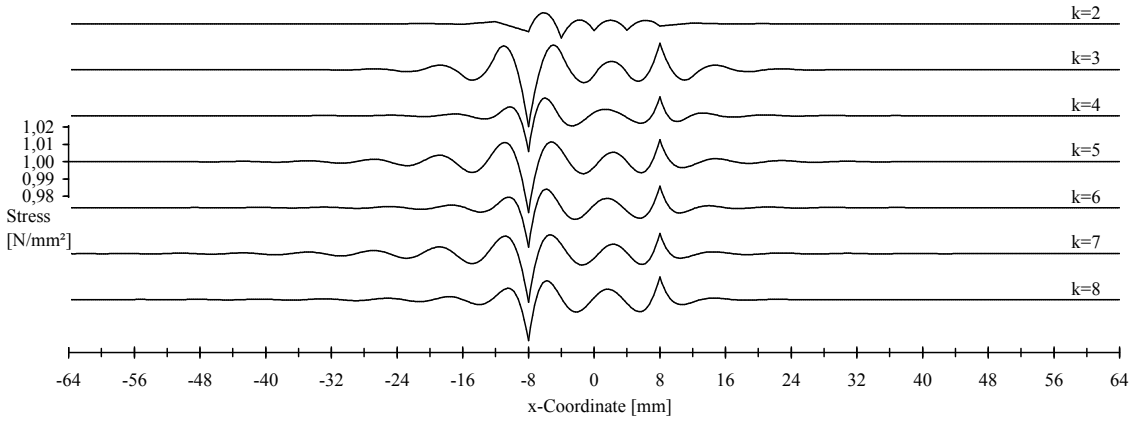

Fig. 7.23: Stress σ_{xx} in finite elements of Section 1-1 for C^0-continuous linear transition of Young's modulus and varying order k of B-Spline finite elements.

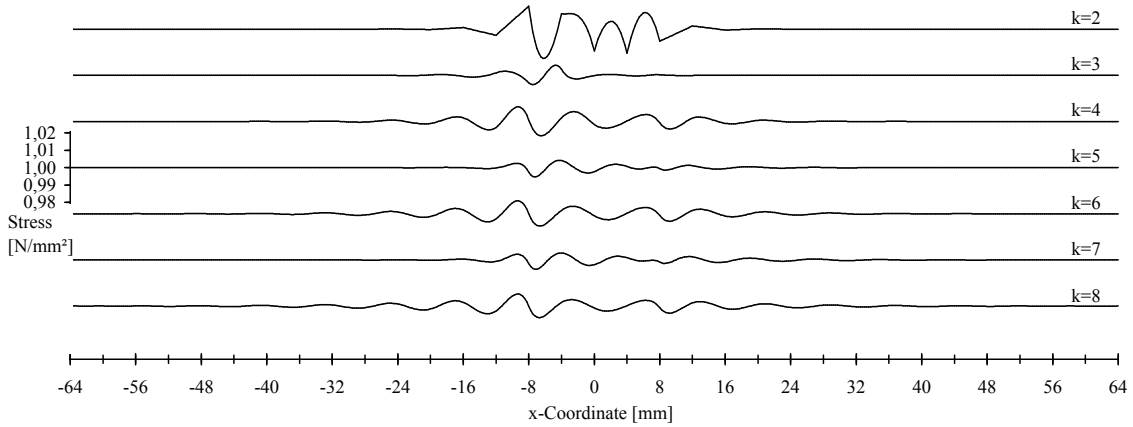

Fig. 7.24: Stress σ_{xx} in finite elements of Section 1-1 for C^1-continuous cubic transition of Young's modulus and varying order k of B-Spline finite elements.

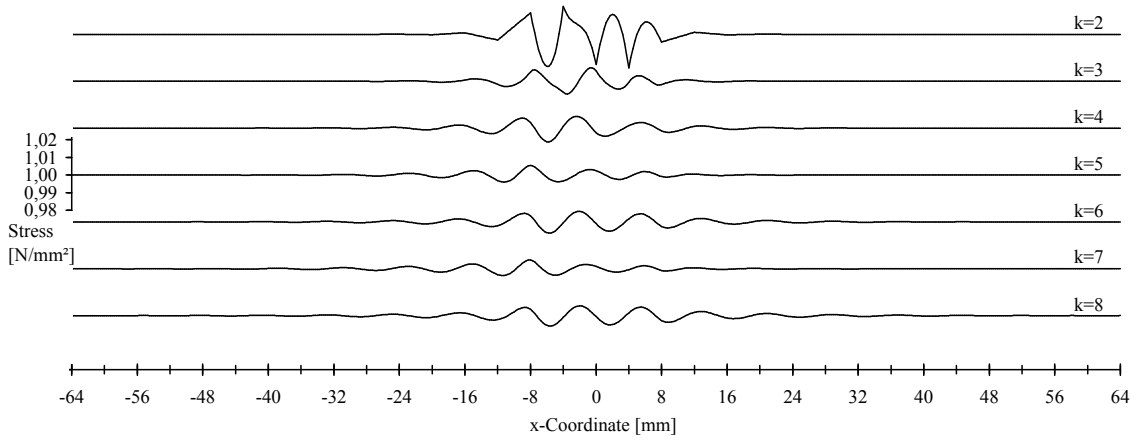

Fig. 7.25: Stress σ_{xx} in finite elements of Section 1-1 for C^2-continuous quintic transition of Young's modulus and varying order k of B-Spline finite elements.

not appear to be relevant. Concluding, for best approximation of material transitions, multiphase B-spline finite elements of order $k = 2$ or $k = 3$ are proposed, as no further improvement can be expected for an increase of k (while the p-version was much more effective for homogeneous problems).

The Figures 7.26 to 7.28 deal with the h-version, namely a change of element number measured in terms of element size h. Fig. 7.26 shows the combination of a linear transition function and B-splines shape functions of order $k = 2$. The stress σ_{xx} converges very effectively with decreasing mesh size. Same effect is observed for the linear transition function and $k = 3$ in Fig. 7.27. Even the discussed defect at $x = -8$ and $x = 8$ decreases, which would not have been clear without this study, but it appears to converge less effectively.

As a further study the combination of cubic transition and $k = 3$ is shown in Fig. 7.28. Without the defect the problem appears to converge even faster then for a linear transition and $k = 2$ with respect to decreasing mesh size h.

As the major conclusion, it is quite obvious that the h-version is much more effective in modeling heterogeneous materials than the p-version. Best results are achieved for simple linear transitions in combination with B-spline functions of order $k = 2$. This supports the statement that a grid-based model with simple bilinear mapping functions is reasonable and a higher-order mapping function will not necessarily lead to essentially improved answers. Only exception is a cubic transition function in combination with B-splines of order $k = 3$. But then it is expected, that in fact the cubic transition function needs to be exactly mapped which is not easy to assure

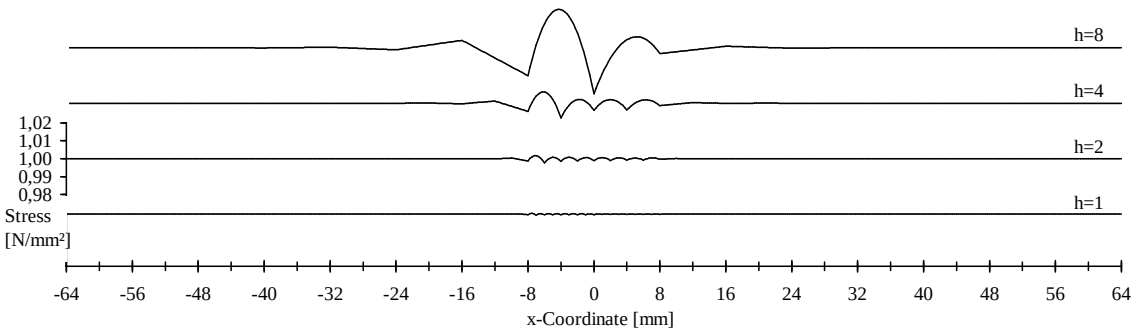

Fig. 7.26: Stress σ_{xx} in finite elements of Section 1-1 for C^0-continuous linear transition of Young's modulus, order k=2 and varying size h of B-Spline finite elements.

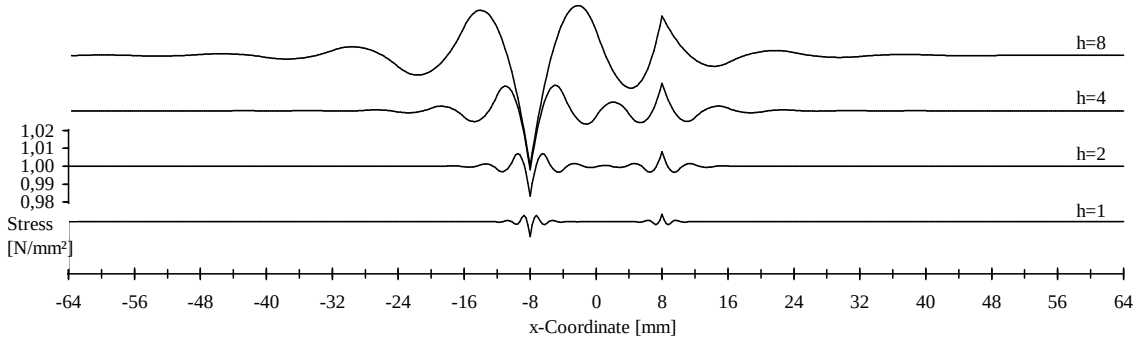

Fig. 7.27: Stress σ_{xx} in finite elements of Section 1-1 for C^0-continuous linear transition of Young's modulus, order k=3 and varying size h of B-Spline finite elements.

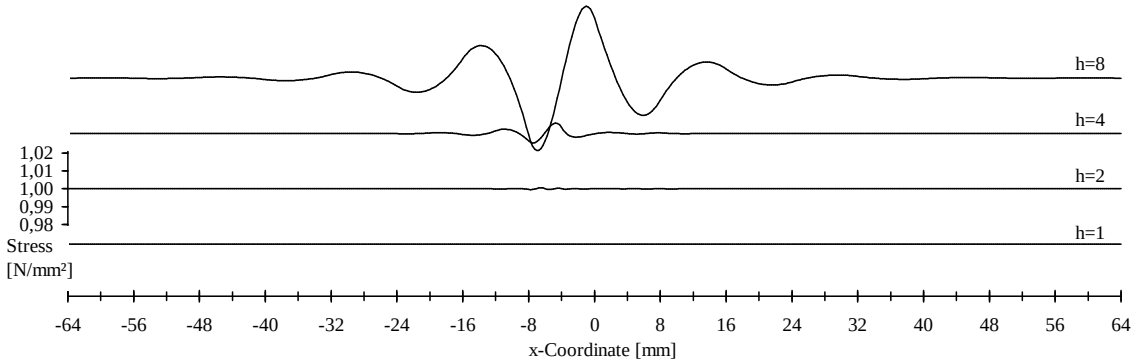

Fig. 7.28: Stress σ_{xx} in finite elements of Section 1-1 for C^1-continuous cubic transition of Young's modulus, order k=3 and varying size h of B-Spline finite elements.

for arbitrary geometries of grid-based models. As a further conclusion it is noted that the dimension of error in all examples is within the acceptable tolerance of a few percent error in stress or essentially below. Again, therefore the method is principally valid to model heterogeneous problems.

In all cases multiphase B-spline finite elements of order $k = 1$ lead to significantly worse results which is only summarized in the following final summaries of error in stress and energy in form of Figs. 7.29 to 7.32. Fig. 7.29 summarizes the maximum error of stress in the p-version and Fig. 7.30 that in the h-version. Similar trends in the error of energy are observed for the p-version and h-version in Figs. 7.31 and 7.32, respectively. It is quite interesting to evaluate the convergence rates of error energy from Fig. 7.32 as assembled in Table 2 and compare them to those of the homogeneous problem.

Error(2h) / Error(h)			
	$h = 4s$	$h = 2s$	$h = 1s$
Linear Transition, $k = 2$	18.041	19.016	18.575
Linear Transition, $k = 3$	6.2506	7.8595	7.9919
Cubic Transition, $k = 2$	10.332	20.836	20.213
Cubic Transition, $k = 3$	107.54	175.00	-

Table 2: Convergence rates of error energy as in Fig. 7.32 and assignment of first row to Fig. 7.26, second row to Fig. 7.27, third row without illustration and fourth row to Fig. 7.28

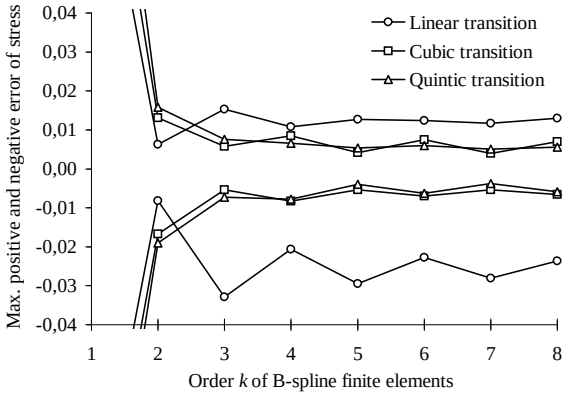

Fig. 7.29: Maximum error of stress in p-version

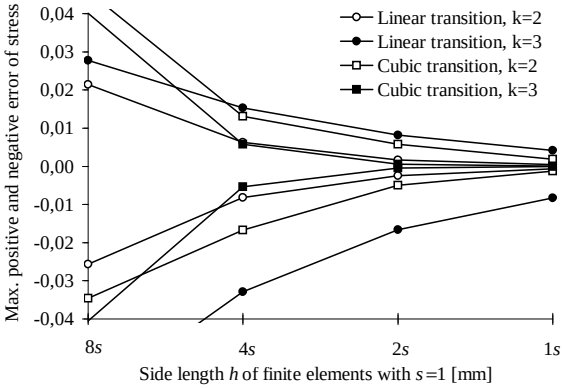

Fig. 7.30: Maximum error of stress in h-version

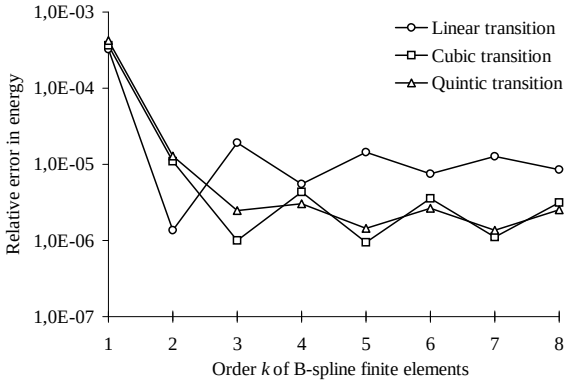

Fig. 7.31: Energy error in p-version

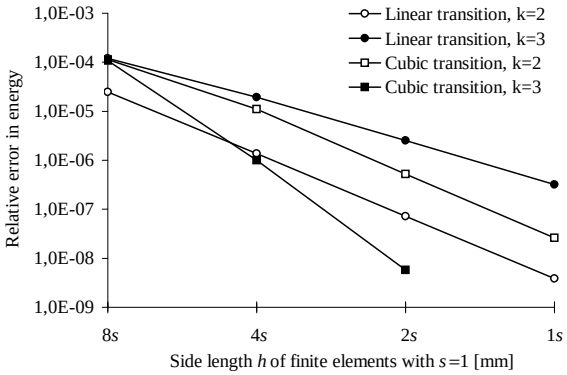

Fig. 7.32: Energy error in h-version

7.7 Overall error estimation

Several examples showed that the presented multiphase B-spline finite elements can be applied to the mechanical analysis of heterogeneous materials and in the h-version lead to good convergence of stress and system energy. These elements were especially designed to reduce severely defective stresses along interfaces of grid-based models. However, therefore a substitute problem was introduced (Section 7.1), which already includes an error in advance. For an accurate assessment of the proposed method, the overall error is considered. This also allows to identify effectively optimal parameter combinations. The following sources of error are considered:

Geometrical error The geometrical error refers to any difference between the heterogeneous material geometry of the original problem and that of the finite element problem. Such a difference can have several reasons such as e.g. imprecise geometrical data of the material, the representation by a grid model or the the introduction of a substitute problem (Section 7.1).

Discretization error The discretization error denotes the classical approximation error which results of the finite functional space of the finite elements. This error evaluates the adequacy of shape functions in the approximation of the exact solution of the posed problem. It is important to note that the discretization refers to the posed problem, which might differ from the intended problem, e.g. by the geometrical error.

Numerical error The term numerical error summarizes several possible error sources. These errors can result from the limited computational precision or from user-defined tolerances

such as in the iterative solution process of the linear equation system. In any case it needs to be assured that the numerical error is essentially below the geometrical error and the discretization error.

In [6] the common basis of error in energy appeared to be most reasonable to compare different sources of error. However, in this context the effect on the stress solution is of relevant interest. In the following the overall error, or effective error, includes the geometrical error and the discretization error. The numerical error is negligible.

The overall error is estimated with regard to the example of one material transition of Section 7.6. The linear material transition is considered in combination with multiphase B-spline finite elements of order $k = 2$. The size of the material transitions zone s_t (D in Fig. 7.21) is variable. Only some assumptions allow for a comparison of geometrical and discretization error. The geometrical error only depends on s_t of the substitute problem. The geometry is exactly mapped onto the elements which are based on a sufficient number of integration points. If $s_t = 0$ the geometry corresponds to the original problem (compare to Section 7.3).

In example of Section 7.6 the analytical stress solution of the substitute problem corresponds to that of the original problem. However, the effective stiffness is changed due to the material transition zone. This can be expressed in error of potential energy. A relative error of the stress is assigned to the square root of relative error of energy. This is an assumption which presumes that the error of stress due to the geometrical error is equally distributed over the domain. The discretization error causes local defects in the stress solution. It follows that an equally distributed error and a maximum local error are of different character. However, Figs. 7.33 and 7.34 illustrate the relationship of these errors where the effective error is the sum of geometrical error and discretization error.

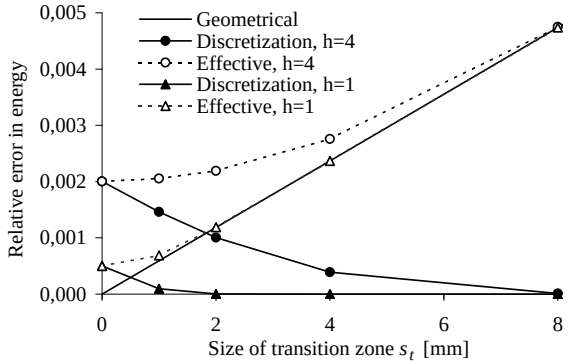

Fig. 7.33: Effective error of energy

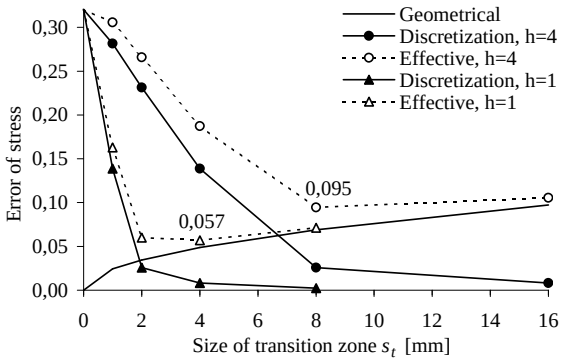

Fig. 7.34: Effective maximum error of stress

With respect to the relative error of energy the introduction of a material transition zone ($s_t > 0$) is always disadvantageous. However, the dimension of the relative geometrical error of 0.5% at $s_t = 8$ in Fig. 7.33 is comparatively low and tolerable. The errors in stress according to Fig. 7.34 are essentially decreased by introduction of the material transition zone in contrast to the original problem ($s_t = 0$). For size $h = 4$ of elements the lowest effective error is achieved for $s_t = 8$, for $h = 1$ it is $s_t = 4$. Also in the effective error of stress the proposed method converges with decreasing mesh size h but less fast as the pure discretization error. However, this is a successful result of the introduced substitute problem. It is highlighted that the number of degrees of freedom connected to a specific mesh size h ($h = 1$ or $h = 4$) in Fig. 7.34 remains unchanged.

8 CONCLUSIONS

This paper provides transparent access to B-spline finite elements by simple one-dimensional examples which are comprehensible by hand calculation. Two-dimensional B-spline finite elements are developed which are of variable order k. In a complex homogeneous problem these elements achieve exemplary convergence rates. They are highly accurate, as tested up to the order $k = 5$. Even with respect to the variable order k, only a few element stiffness matrices are required to create and solve the global finite element problem on a uniform grid. By the use of iterative solvers a global stiffness matrix needs not to be stored such that the memory demand can be reduced to a minimum of essentially required vectors. Moreover, the presented element-based modelling on uniform grids is ideally suited for an effective use of the multigrid method.

The multiphase finite element concept extends the B-spline finite elements of variable order k to their application in the mechanical analysis of heterogeneous solids. Several advantages of grid-based modelling are maintained such that the extension to three-dimensional modelling of heterogeneous solids remains straightforward. The geometrical description of different phases within the material is independent of the finite element mesh. Surfaces of the phases need not to be defined as usually required in aligned meshing. The geometry can originate from pixel models or exact mapping of material functions within the finite elements. As an essential key, an original problem with material discontinuities is replaced by a substitute problem with continuous material approximations. The errors of stress and energy are analyzed with respect to B-spline order k, element size h, as well as type of material transition function and size s_t of material transition zone. Therefore best parameter combinations of this method can be identified.

In contrast to homogeneous materials where an increase of B-spline order k is optimal (p-version), for heterogeneous materials convergence is almost only achieved by refining the mesh (h-version). Apart from the considerate use of cubic B-spline finite elements for heterogeneous materials, bilinear material transition functions in combination with quadratic B-spline finite elements appear optimal and robust. An ideal size of the material transition zone is approximately assigned to the size of two to four elements ($2h$ to $4h$). Finally, the effective error, as sum of discretization error and geometrical error, from the substitute problem is estimated. Also for the effective error the substitute problem leads to a successful trade-off. While the effective energy error only slightly increases, severe errors in the stress solution effectivly decrease by an essential magnitude. Although the effective error of stress converges less fast than the pure discretization error within the substitute problem, the presented method establishes a substantial improvement for grid-based modelling. Therefore multiphase B-spline finite elements are proposed as novel alternative in the mechanical analysis of heterogeneous solids.

REFERENCES

[1] K.-J. Bathe. *Finite Element Procedures*. Prentice Hall, Englewood Cliffs, 1996.

[2] C. De Boor. *A practical guide to splines*. Springer, New York, USA, 1978.

[3] A. Duschek. *Vorlesungen über höhere Mathematik*. Springer, Wien, Austria, 1961.

[4] S. Häfner, S. Eckardt, and C. Könke. A geometrical inclusion-matrix model for the finite element analysis of concrete at multiple scales. In K. Gürlebeck, L. Hempel, and C. Könke, editors, *Proc. IKM 2003*, Weimar, Germany, 2003.

[5] S. Häfner, S. Eckardt, T. Luther, and C. Könke. Mesoscale modeling of concrete: Geometry and numerics. *Computers and Structures*, 84(7):450–461, 2006.

[6] S. Häfner and C. Könke. A multigrid finite element method for the mesoscale analysis of concrete. In P. Neittaanmäki, T. Rossi, K. Majava, and O. Pironneau, editors, *Proc. ECCOMAS 2004*, Jyväskylä, Finland, 2004.

[7] S. Häfner and C. Könke. Damage simulation of heterogeneous solids by nonlocal formulations on orthogonal grids. In K. Gürlebeck and C. Könke, editors, *Proc. IKM 2006*, Weimar, Germany, 2006.

[8] S. Häfner and C. Könke. Multigrid preconditioned conjugate gradient method in the mechanical analysis of heterogeneous solids. In K. Gürlebeck and C. Könke, editors, *Proc. IKM 2006*, Weimar, Germany, 2006.

[9] M. R. Hestenes and E. L. Stiefel. Methods of conjugate gradients for solving linear systems. *J. Res. Nat. Bur. Standards Sect.*, 49(5):409–439, 1952.

[10] K. Höllig. *Finite Element Methods with B-Splines*. SIAM, Philadelphia, 2003.

[11] K. Höllig, U. Reif, and J. Wipper. Multigrid methods with web-splines. *Numerische Mathematik*, 91(2):237–256, 2002.

[12] M. Kachanov, B. Shafiro, and I. Tsukrov. *Handbook of elasticity solutions*. Kluwer Academic Publishers, Dordrecht, Netherlands, 2003.

[13] M. Kessel. B-Spline basierte Scheibenelemente für rechteckige Gebiete. Seminar paper, Institute of Structural Mechanics, Bauhaus University Weimar, 2004.

[14] M. Kessel. Implementierung rechteckiger Scheibenelemente mit B-Spline Ansätzen n-ter Ordnung. Diploma thesis, Institute of Structural Mechanics, Bauhaus University Weimar, 2005.

[15] V.V. Meleshko. Selected topics in the history of the two-dimensional biharmonic problem. *Appl. Mech. Rev.*, 56(1):33–85, 2003.

[16] L. L. Mishnaevsky and S. Schmauder. Continuum mesomechanical finite modeling in materials development: a state-of-the-art-review. *Applied Mechanics Reviews*, 54(1):49–69, 2001.

[17] H. Schwetlick and H. Kretzschmar. *Numerische Verfahren für Naturwissenschaftler und Ingenieure*. Fachbuchverlag, Leipzig, 1991.

[18] T. Steinkopff, M. Sautter, and J. Wulf. Mehrphasige Finite Elemente in der Verformungs- und Versagensanalyse grod mehrphasiger Werkstoffe. *Archive of Applied Mechanics*, 65(7):496–506, 1995.

[19] O.C. Zienkiewicz and R.L. Taylor. *The finite element method, Fourth Edition, Volume 1, Basic formulation and linear problems*. McGraw-Hill, UK, 1997.

[20] T. Zohdi and P. Wriggers. *Introduction to Computational Micromechanics*. Springer, Berlin, 2005.

[21] T.I. Zohdi. Computational optimization of the vortex manufacturing of advanced materials. *Comput. Methods Appl. Mech. Engrg.*, 190:6231–6256, 2001.